AMERICAN SOCIETY FOR MICROBIOLOGY | Journal of Virology®

VIRUS-CELL INTERACTIONS

Allosteric HIV-1 Integrase Inhibitors Lead to Premature Degradation of the Viral RNA Genome and Integrase in Target Cells

Michaela K. Madison,[a] Dana Q. Lawson,[a] Jennifer Elliott,[a] Ayşe Naz Ozantürk,[b] Pratibha C. Koneru,[c,d] Dana Townsend,[a] Manel Errando,[e] Mamuka Kvaratskhelia,[c,d] Sebla B. Kutluay[a]

Department of Molecular Microbiology, Washington University School of Medicine, Saint Louis, Missouri, USA[a]; Department of Molecular Biology and Genetics, Bilkent University, Ankara, Turkey[b]; Center for Retrovirus Research[c] and College of Pharmacy,[d] The Ohio State University, Columbus, Ohio, USA; Department of Physics, Washington University, Saint Louis, Missouri, USA[e]

ABSTRACT Recent evidence indicates that inhibition of HIV-1 integrase (IN) binding to the viral RNA genome by allosteric integrase inhibitors (ALLINIs) or through mutations within IN yields aberrant particles in which the viral ribonucleoprotein complexes (vRNPs) are eccentrically localized outside the capsid lattice. These particles are noninfectious and are blocked at an early reverse transcription stage in target cells. However, the basis of this reverse transcription defect is unknown. Here, we show that the viral RNA genome and IN from ALLINI-treated virions are prematurely degraded in target cells, whereas reverse transcriptase remains active and stably associated with the capsid lattice. The aberrantly shaped cores in ALLINI-treated particles can efficiently saturate and be degraded by a restricting TRIM5 protein, indicating that they are still composed of capsid proteins arranged in a hexagonal lattice. Notably, the fates of viral core components follow a similar pattern in cells infected with eccentric particles generated by mutations within IN that inhibit its binding to the viral RNA genome. We propose that IN-RNA interactions allow packaging of both the viral RNA genome and IN within the protective capsid lattice to ensure subsequent reverse transcription and productive infection in target cells. Conversely, disruption of these interactions by ALLINIs or mutations in IN leads to premature degradation of both the viral RNA genome and IN, as well as the spatial separation of reverse transcriptase from the viral genome during early steps of infection.

IMPORTANCE Recent evidence indicates that HIV-1 integrase (IN) plays a key role during particle maturation by binding to the viral RNA genome. Inhibition of IN-RNA interactions yields aberrant particles with the viral ribonucleoprotein complexes (vRNPs) eccentrically localized outside the conical capsid lattice. Although these particles contain all of the components necessary for reverse transcription, they are blocked at an early reverse transcription stage in target cells. To explain the basis of this defect, we tracked the fates of multiple viral components in infected cells. Here, we show that the viral RNA genome and IN in eccentric particles are prematurely degraded, whereas reverse transcriptase remains active and stably associated within the capsid lattice. We propose that IN-RNA interactions ensure the packaging of both vRNPs and IN within the protective capsid cores to facilitate subsequent reverse transcription and productive infection in target cells.

KEYWORDS ALLINIs, capsid, HIV-1, integrase, maturation, protein-RNA interaction, RNA packaging, TRIM5, reverse transcriptase

Received 18 May 2017 **Accepted** 23 May 2017

Accepted manuscript posted online 14 June 2017

Citation Madison MK, Lawson DQ, Elliott J, Ozantürk AN, Koneru PC, Townsend D, Errando M, Kvaratskhelia M, Kutluay SB. 2017. Allosteric HIV-1 integrase inhibitors lead to premature degradation of the viral RNA genome and integrase in target cells. J Virol 91:e00821-17. https://doi.org/10.1128/JVI.00821-17.

Editor Wesley I. Sundquist, University of Utah

Address correspondence to Sebla B. Kutluay, kutluay@wustl.edu.

M.K.M. and D.Q.L. are co-first authors.

The genesis of infectious HIV-1 particles is a multistep process orchestrated by the HIV-1 polyproteins Gag and Gag-Pol. Recruitment of a single viral RNA genome dimer by a small number of Gag molecules to the plasma membrane nucleates the assembly of thousands of Gag and hundreds of Gag-Pol molecules into an immature virion (1). Thereafter, cleavage of Gag and Gag-Pol polyproteins by the virally encoded protease enzyme liberates these polyproteins to their constituent domains, triggering virion maturation. In mature virions, the cleaved nucleocapsid (NC) domain of Gag condenses with the viral RNA (vRNA) genome inside the conical core, composed of the capsid (CA) protein (1). Importantly, RNA (viral or cellular) has been shown to play a structural role in viral particles (2, 3). Although the proposed models of virion maturation have been largely centered on proteolytic cleavage events of Gag, recent studies have revealed an active role of integrase (IN) in encapsidation of the viral RNA genome within the mature conical CA lattice (4).

Early mutagenesis screens of IN have demonstrated that certain mutations, collectively referred to as class II IN mutations, are pleiotropic and adversely affect particle assembly, maturation, and reverse transcription (5–16). Interestingly, deletion of IN and certain class II IN mutations leads to profound morphological defects in virions. In these particles, the viral ribonucleoprotein complexes (vRNPs), mainly composed of the viral genomic RNA and NC, are eccentrically localized between the empty CA lattice and the viral membrane (7, 9, 17). A remarkably similar morphological defect is observed in particles generated in the presence of allosteric integrase inhibitors (ALLINIs) (also known as LEDGINs, NCINIs, or INLAIs) (18–23). Proposed mechanisms that underlie this morphogenesis defect include ALLINI-induced aberrant IN multimerization (9, 17, 24–27) and inhibition of IN binding to the viral RNA genome (4).

While a large fraction of eccentric particles contain irregularly shaped nonconical CA assemblies (9, 17, 24), they appear to retain all of the components necessary for reverse transcription, i.e., a dimeric viral RNA genome primed with tRNA-Lys, functional reverse transcriptase (RT) (23), and normal levels of NC-RNA complexes (4, 17). Nevertheless, these particles are blocked at an early reverse transcription stage in target cells (9, 11, 13, 24), the basis of which remains unknown. An anticipated, but currently untested, possibility is that in addition to the vRNPs, other components of the viral core (i.e., RT and IN) are mislocalized in eccentric particles and encounter unexpected fates in target cells.

From a different perspective, examination of how eccentric particles behave in infected cells may broaden our understanding of early postentry events, including viral uncoating, reverse transcription, and TRIM5 restriction. Optimal stability of the CA lattice and its timely uncoating have previously been proposed to be important for reverse transcription (28–35). Nevertheless, higher-order CA structures must still exist in cells because the host restriction factor TRIM5 recognizes structural features that exist only in viral cores but not in individual CA monomers (36–39). However, the presence of a conical core is likely not necessary for TRIM5 restriction, as a CA-NC cleavage mutant that does not form conical cores can efficiently saturate TRIM5 restriction (40), and TRIM5 can form lattices around hexameric CA-NC assemblies *in vitro* (41). As such, determining whether the aberrantly formed CA lattices in eccentric particles are stable in target cells despite lack of reverse transcription and whether they can be recognized by TRIM5 proteins will further our knowledge of not only the morphological defects in eccentric particles, but also early viral postentry events.

In this study, we set out to determine why eccentric particles, generated in the presence of ALLINIs or through mutations within IN are blocked at an early reverse transcription stage in target cells. Furthermore, we wanted to examine whether the nonconical CA lattice in the eccentric particles retains features that can be recognized by a restricting TRIM5 protein. Here, we provide compelling evidence that upon infection of target cells, eccentrically localized viral RNA genomes, as well as IN, are prematurely degraded in a proteasome-independent manner, whereas RT remains active and stably associated with the CA lattice. Importantly, neither the total number of NC-RNA complexes nor the footprint of NC on viral RNAs is affected in particles

generated in the presence of ALLINIs. Notably, the CA lattice in eccentric particles can efficiently saturate and be degraded by a restricting TRIM5 protein, suggesting that CA proteins are organized in a hexagonal lattice despite the morphological aberrations. Overall, our findings suggest that spatial separation of RT from vRNPs and premature degradation of the viral RNA genome in target cells underlie the reverse transcription defect of eccentric particles in target cells. We propose that IN-RNA interactions mediate correct localization of the viral RNA genome, RT, and IN within the CA lattice to prevent their premature degradation in target cells.

RESULTS

Effects of BI-B2 treatment on the fates of core components in target cells. To determine why eccentric viral particles, generated in the presence of ALLINIs, fail to support reverse transcription in target cells, we monitored the fates of eccentric particle components in infected cells. To this end, we took advantage of a previously developed elaborate approach with which we biochemically tracked multiple core components in infected cells (42). In brief, pgsA-745 or pgsA-745-derived cells stably expressing a nonrestricting human TRIM5α (huTRIM5α) protein were synchronously infected at 4°C with mock- or BI-B2-treated particles. Note that we chose to primarily work with pgsA-huTRIM5α cells, as they are equally permissive to HIV-1 replication as the unmodified pgsA-745 cells (42) and served as a matched control for the studies involving restricting TRIM5 proteins detailed below. Following infections, postnuclear material was harvested either immediately after virus binding ($T = 0$) or after 2 h of incubation at 37°C ($T = 2$ h) and was separated by size on linear sucrose gradients. The collected fractions were analyzed by immunoblotting for the viral proteins IN and CA, as well as quantitative-PCR (Q-PCR)-based assays for viral RNA, cDNA, and RT activity.

In line with previous studies (43), wild-type (WT) particles generated in the presence of BI-B2 exhibited a nearly 10-fold infectivity defect (Fig. 1A), whereas the HIV-$1_{A128T\ IN}$ mutant virus was markedly resistant to BI-B2 (Fig. 1A). As expected, BI-B2 treatment did not affect the binding of virions to cells, as similar levels of CA (Fig. 1B), IN (Fig. 1B), and vRNA (Fig. 1C) were present primarily in sucrose fractions 6 to 8 for both mock- and BI-B2-treated particles, representing virions that are bound to plasma membrane fragments of various sizes. In contrast, analysis of viral core components at 2 hours postinfection revealed remarkably different fates for the components of mock- and BI-B2-treated particles. As previously observed (42), for mock-treated particles, a large fraction of CA was detected in the top two fractions (Fig. 1D), representing soluble CA that either was not assembled into viral cores (44) or had uncoated. A smaller population of CA was present in the denser fractions, representing the larger reverse transcription complexes (Fig. 1D). Notably, comparable levels and distribution patterns of CA were detected in sucrose fractions for BI-B2-treated particles (Fig. 1D). While IN and vRNA comigrated with CA in the dense fractions for mock-treated particles (Fig. 1D and E), BI-B2 treatment led to a nearly complete loss of IN and a significant reduction in vRNA in the dense fractions without a concurrent increase in the top fractions containing soluble RNAs and proteins (Fig. 1D and E). These changes were accompanied by a similar degree of reduction in reverse transcription products (Fig. 1F).

To ensure that degradation of IN and RNA was not due to overexpression of huTRIM5α or an indirect effect of BI-B2 treatment, we conducted similar experiments in unmodified pgsA cells using the BI-B2-resistant HIV-$1_{A128T\ IN}$ mutant virus (Fig. 1A) (43). In line with the above-described findings, BI-B2 treatment of neither HIV-1_{WT} nor HIV-$1_{A128T\ IN}$ affected the levels and behavior of CA protein in sucrose gradients (Fig. 1G). In contrast, while BI-B2 treatment of WT particles significantly reduced the levels of IN (Fig. 1G) and vRNA (Fig. 1H) in dense fractions, BI-B2 treatment of HIV-$1_{A128T\ IN}$ had no discernible effect on the levels or the migration patterns of IN and vRNA (Fig. 1G and H). Notably, analysis of RT activity in sucrose fractions revealed that a large fraction of RT comigrated with the larger CA-containing complexes and that BI-B2 treatment of WT particles had no effect on the migration behavior of RT (Fig. 1I). These results collec-

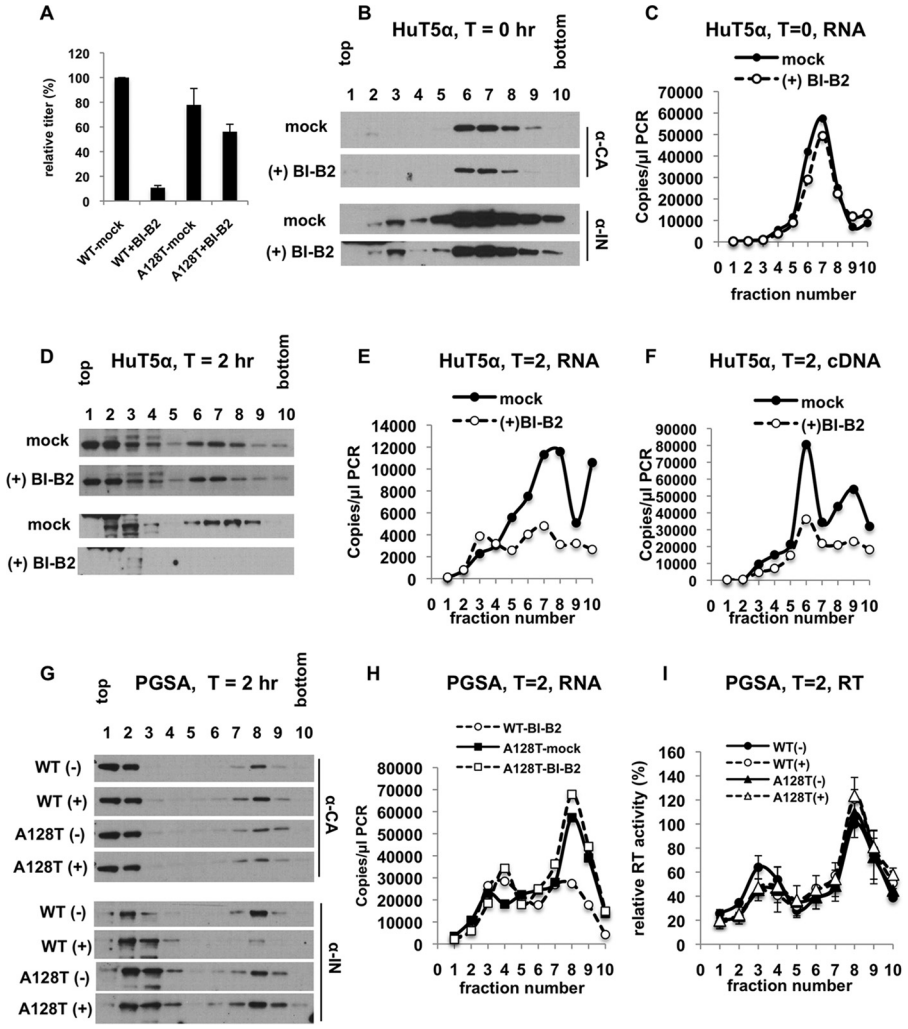

FIG 1 Fates of BI-B2-treated core components in target cells. (A) pgsA cells were infected in parallel with mock- or BI-B2-treated VSV-G-pseudotyped GFP reporter HIV-1_{WT} and HIV-$1_{A128T\ IN}$. Virus titers were determined 2 days postinfection (dpi) by FACS, and the titer of mock-treated WT virus was set to 100%. (B to F) pgsA-huTRIM5α cells were infected with mock- or BI-B2-treated HIV-1_{WT}/VSV-G. Infected cells were processed at 0 h and 2 h as explained in Materials and Methods. (B and C) Western blot analysis of CA (p24) and IN (B) and Q-RT-PCR analysis of viral RNA (C) in fractions collected from 0-h samples. (D to F) Western blot analysis of CA and IN (D) and Q-RT-PCR analysis of viral RNA (E) and reverse transcription products (F) in fractions collected from 2-h samples. (G to I) pgsA cells were infected with mock- or BI-B2-treated HIV-1_{WT}/VSV-G or HIV-$1_{A128T\ IN}$/VSV-G. The infected cells were processed at 2 h as described above. (G and H) Western blot analysis of CA (p24) and IN (G) and Q-PCR analysis of viral RNA (H). The data are representative of the results of at least two independent experiments. (I) RT activity in collected fractions was analyzed by a Q-PCR assay. Peak RT activity (i.e., in the 8th fraction) of mock-treated WT samples was set to 100%. The data represent the averages of the results of two independent experiments; the error bars show the ranges.

tively indicate that BI-B2 treatment of WT particles specifically leads to degradation of IN and vRNA, as well as the spatial separation of RT from vRNPs in target cells.

Effects of BI-D treatment on fates of core components in target cells. To test whether the above-described effects on viral core components were a general property of ALLINIs, we conducted similar experiments with another ALLINI, BI-D, in pgsA-huTRIM5α and unmodified pgsA cells. In line with the above-mentioned findings, although BI-D treatment of WT particles had no effect on the migration pattern or the levels of CA (Fig. 2A and D), it led to significantly lower levels of IN (Fig. 2A and D), vRNA (Fig. 2B and E), and cDNA (Fig. 2C and F) in dense sucrose fractions. Importantly, similar amounts of RT comigrated with CA in the dense fractions for both mock- and BI-D-treated particles (Fig. 2G), suggesting its retention within the larger CA complexes.

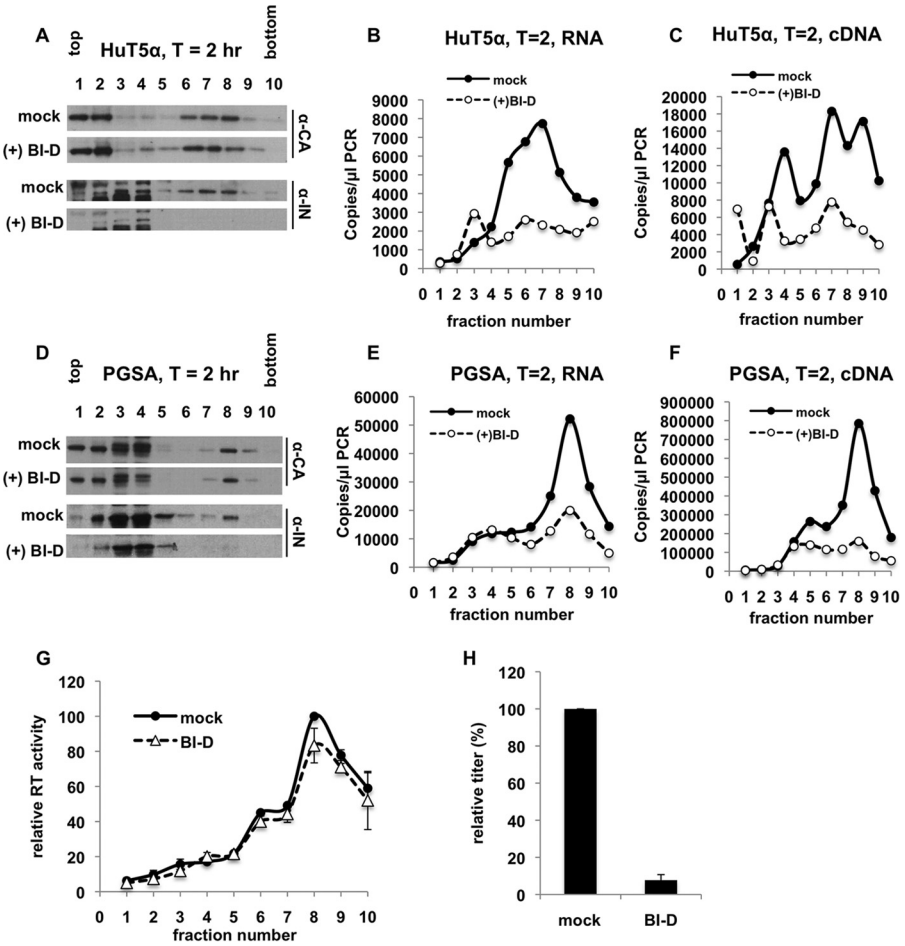

FIG 2 Fates of BI-D-treated core components in target cells. (A to F) pgsA-huTRIM5α (A to C) or unmodified pgsA (D to F) cells were infected with mock- or BI-D-treated VSV-G-pseudotyped GFP reporter HIV-1_{WT}. The infected cells were processed at 2 h as explained in Materials and Methods. Western blot analysis of CA (p24) and IN (A and D) and Q-RT-PCR analysis of viral RNA (B and E) and reverse transcription products (C and F) in the collected fractions are shown. The data are representative of the results of at least two independent experiments. (G) RT activity in fractions collected from pgsA-huTRIM5α cells infected with BI-D-treated HIV-1_{WT}/VSV-G were analyzed by a Q-PCR-based assay. Peak RT activity (i.e., in the 8th fraction) of mock-treated samples was set to 100%. The data represent the averages of two independent experiments; the error bars show the ranges. (H) Titers of mock- and BI-D-treated viruses on pgsA-huTRIM5α cells were determined by FACS, and the titer of mock-treated WT virus was set to 100%. The data represent the means and standard deviations (SD) of the results of three independent experiments.

Degradation and spatial separation of viral core components in BI-D-treated particles were accompanied by an expected defect in infectivity (Fig. 2H). These results collectively indicate that degradation of vRNA and IN and separation of RT from vRNPs are common outcomes of ALLINI treatment.

Fates of HIV$_{IN\ R269A/K273A}$ core components in target cells. We next extended these experiments to the R269A/K273A class II IN mutant, which specifically inhibits IN binding to the viral RNA genome without affecting the catalytic activity of IN and leads to formation of particles with the eccentric morphology (4). Although the nearby K264A/K266A mutation similarly inhibits IN-RNA interactions and generates eccentric particles, this mutation is pleiotropic and interferes with the catalytic activity of IN. As such, we decided to focus on the R269A/K273A mutant in this study.

pgsA-huTRIM5α and pgsA cells were infected with HIV-1_{WT} and HIV-$1_{IN\ R269A/K273A}$ viruses, and cell lysates were analyzed following separation on sucrose gradients as described above. As expected, the R269A/K273A IN mutation did not affect virion binding to pgsA-huTRIM5α cells, as revealed by similar levels and distribution patterns of CA (Fig. 3A), IN (Fig. 3A), vRNA (Fig. 3B), and RT (Fig. 3C) in the sucrose gradient. At

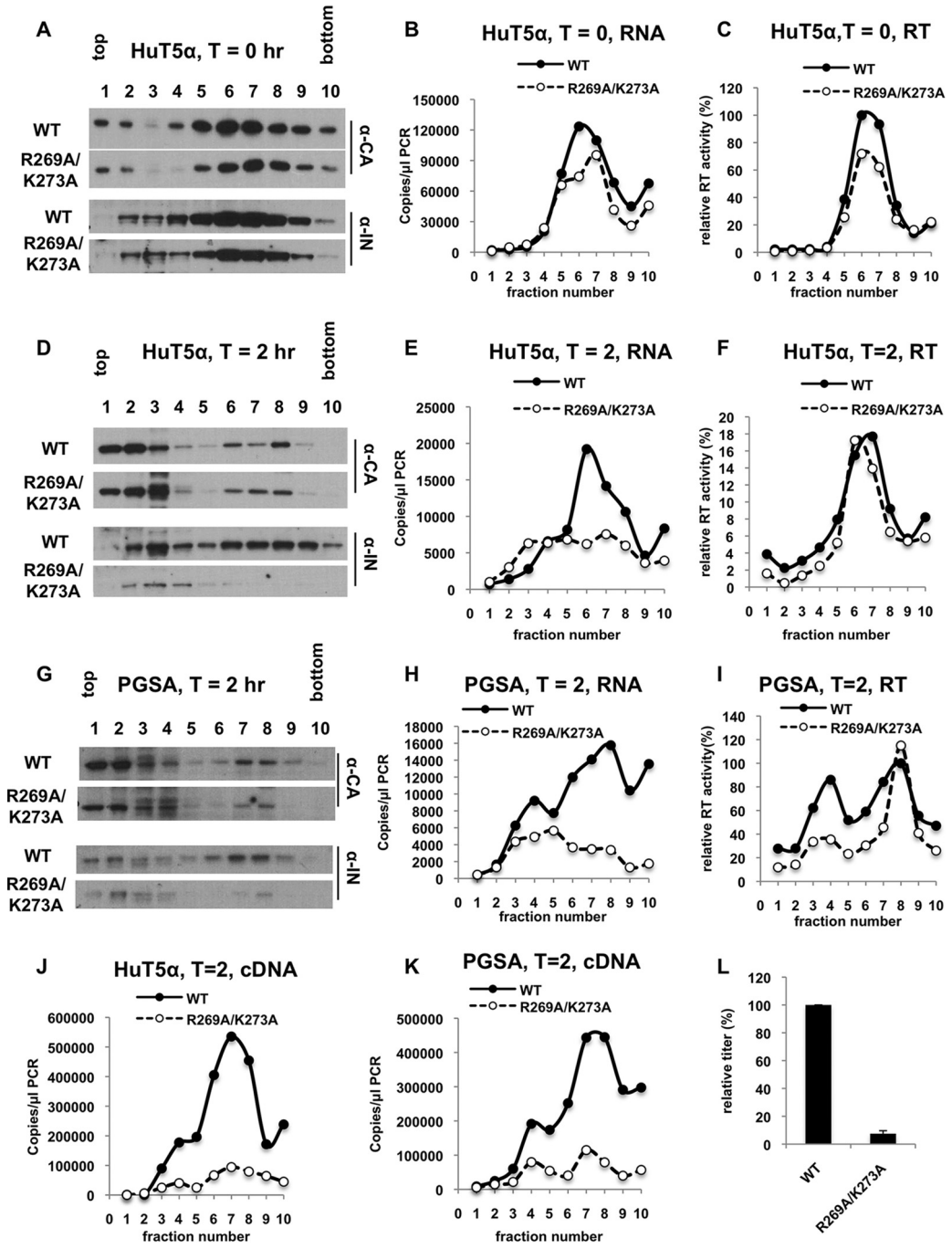

FIG 3 Fates of HIV-1_{WT} and HIV-$1_{IN\ R269A/K273A}$ core components in target cells. pgsA-huTRIM5α or unmodified pgsA cells were infected in parallel with VSV-G-pseudotyped GFP reporter HIV-1_{WT} or HIV-$1_{IN\ R269A/K273A}$. The infected cells were processed at 0 h and 2 h as explained in Materials and Methods. (A to C) Western blot analysis of CA (p24) and IN (A) and Q-PCR analysis of viral RNA (B) and RT activity (C) in fractions collected at 0 h postinfection of pgsA-huTRIM5α cells. (D to F) Western blot analysis of CA and IN (D) and Q-PCR analysis of viral RNA (E) and RT activity (F) in fractions collected from 2 h postinfection of pgsA-huTRIM5α cells. (G to I) Western blot analysis of CA and IN (G) and Q-PCR analysis of viral RNA (H) and RT activity (I) in fractions collected from 2 h postinfection of pgsA cells. (J and K) Q-PCR analysis of reverse transcription products (cDNA) in fractions collected from pgsA-huTRIM5α (J) or pgsA (K) cells. The data are representative of the results of at least two independent experiments. (L) pgsA-huTRIM5α cells were infected as described above, and virus titers were determined at 2 dpi by FACS analysis. The data represent the means of two biological replicates. The error bars represent the ranges.

2 h postinfection, no detectable difference in the amount and distribution of CA was observed for HIV-1_{WT} and HIV-$1_{IN\ R269A/K273A}$ particles (Fig. 3D). In contrast, the IN R269A/K273A mutation led to nearly complete loss of IN (Fig. 3D) and a large reduction in vRNA (Fig. 3E) in dense sucrose fractions. Lack of a corresponding increase in top

fractions containing soluble proteins and RNA likely indicates that viral RNA and IN from eccentric particles are degraded. In line with the above-mentioned findings, similar levels of RT comigrated with CA in the dense sucrose fractions for both WT and mutant particles (Fig. 3F). Importantly, similar experiments conducted in pgsA cells also revealed that IN and vRNA in HIV-$1_{IN\ R269A/K273A}$ particles were degraded (Fig. 3G and H), whereas similar levels of CA and RT remained in dense sucrose fractions (Fig. 3G and I). As expected, a reverse transcription (Fig. 3J and K) and subsequent infectivity (Fig. 3L) defect accompanied the degradation of vRNA and separation of RT from vRNPs. Collectively, these results indicate that degradation of vRNA, together with separation of RT from vRNPs, contributes to the reverse transcription defect of eccentric particles in target cells.

Importantly, the results shown in Fig. 1 to 3 were highly reproducible across multiple independent experiments, as exemplified by Q-PCR data showing degradation of vRNA (Fig. 4A and B) and the reverse transcription defect (Fig. 4C and D) of eccentric particles. Analysis of RNA degradation in MT4 cells infected with NL4-3-based full-length viruses similarly revealed that a significant fraction of eccentrically localized viral genomes were degraded prematurely by 2 h following infection (Fig. 4E).

Multimeric state and localization of IN in eccentric particles. Given that IN in eccentric particles is degraded in target cells (Fig. 1 to 3), we reasoned that its localization in particles might be altered. To test this, we fractionated particle components from ALLINI-treated WT virions and HIV-$1_{IN\ R269A/K273A}$ particles using sucrose gradient fractionation following brief detergent treatment and analyzed the migration patterns of CA, IN, and matrix protein (MA) by immunoblotting. It is important to note that comparison of ALLINIs with the R269A/K273A IN mutation is particularly informative for delineating whether premature degradation of vRNA and IN is a consequence of the aberrant IN multimerization or the inability of IN to bind vRNA. While ALLINIs both induce aberrant IN multimerization (9, 17, 24–26) and block IN-RNA interactions (4), the R269A/K273A substitutions impair the ability of IN to bind to vRNA in virions without altering its multimeric state *in vitro* (4).

Upon separation, CA from WT virions migrated as two separate populations, with the majority of CA in the top two fractions (1 and 2) and a smaller amount in fractions 7 to 9 (Fig. 5A). In line with previous findings that CA in eccentric particles migrates in less dense sucrose fractions due to the lack of vRNPs (24, 26), analysis of cores isolated from ALLINI-treated and HIV-$1_{IN\ R269A/K273A}$ particles revealed significantly less CA in the dense sucrose fractions (Fig. 5A) due to the loss of vRNPs (9, 17). For example, while the CA signal in dense fractions peaked in the 8th and 9th fractions, the peak of CA signal in eccentric particles was shifted toward the 7th and 8th fractions (Fig. 5B). As expected, membrane-bound MA remained in the soluble fractions following lysis of WT and eccentric particles (Fig. 5C).

Surprisingly, while WT IN comigrated with CA in dense fractions, R269A/K273A IN was primarily present in the top, soluble-protein-containing fractions (Fig. 5D). Interestingly, IN in BI-D- and BI-B2-treated particles largely migrated in the bottom fractions, although a higher level of soluble IN in BI-D-treated particles was visible (Fig. 5D). The migration behavior of ALLINI-treated IN is in line with a previous study that demonstrated that IN and RT in particles generated in the presence of ALLINI, GS-B, comigrates with the less dense CA cores (24). Possible explanations for the migration behavior of IN in ALLINI-treated particles include its retention within the CA lattice or formation of large IN aggregates outside or loosely associated with the CA lattice. Given that IN in ALLINI-treated particles is degraded similarly to R269A/K273A IN (Fig. 1A and G and 2A and D), we propose that the latter is a more likely possibility.

To better understand the differential migration patterns of IN described above, we employed a complementary dynamic-light-scattering (DLS) approach to evaluate the sizes of corresponding recombinant protein multimers *in vitro* (Fig. 5E). No large particles were detected with untreated WT or R269A/K273A IN molecules, indicating that the R269A/K273A substitutions did not induce higher-order multimerization of IN.

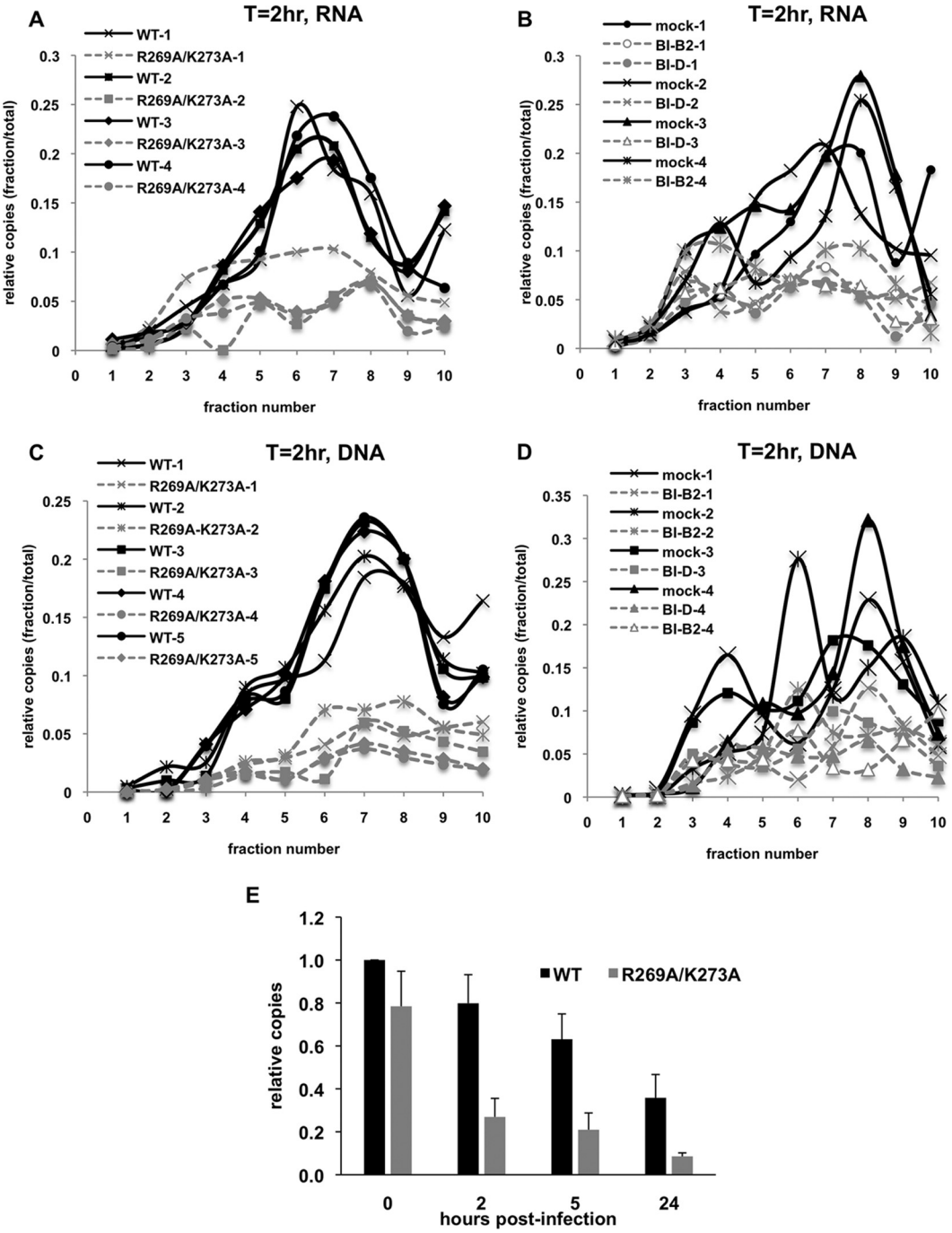

FIG 4 Reproducibility across multiple experiments and in infected MT-4 cells. (A to D) pgsA-huTRIM5α or unmodified pgsA cells infected with eccentric particles and processed as described in Materials and Methods were analyzed for degradation of viral RNA (A and B) and lack of reverse transcription products (C and D). The Q-PCR signal (copies per microliter) in each fraction was divided by the sum of the copy numbers in all the fractions to enable representation of independent experiments on the same graph. (E) MT4 cells were infected with HIV-1_{NL4-3}/VSV-G or HIV-$1_{NL4-3\ IN\ R269A/K273A}$/VSV-G in the presence of 25 μM nevirapine as described above. Q-PCR analysis of viral RNA at the indicated time points postinfection is presented. The data represent means and SD; $n = 4$ biological replicates.

In contrast, addition of BI-D or BI-B2 to WT IN led to the formation of large aggregates with different sizes, ~150 and 950 nm, respectively (Fig. 5E). These findings coupled with previous observations that WT but not R269A/K273A IN binds viral RNA (4) help to explain the differential migration patterns of these proteins: WT IN is part of a large nucleoprotein complex inside the CA core, whereas the mutant IN migrates as a

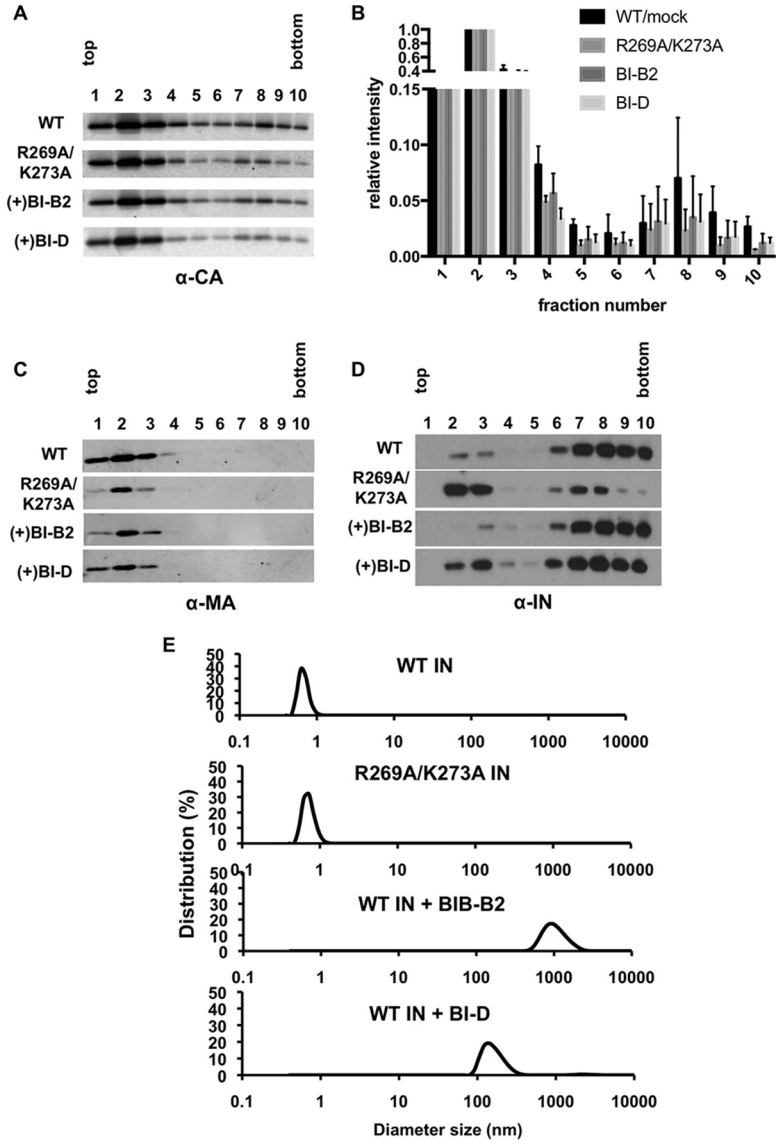

FIG 5 Localization of viral core components in WT and eccentric particles. (A to D) WT, IN R269A/K273A mutant, and BI-B2- and BI-D-treated particles were subjected to equilibrium density centrifugation following lysis in 0.5% Triton X-100. Western blot analyses of CA (A), MA (C), and IN (D) in the collected fractions are shown. (B) Quantitation of the CA Western blots. CA signal for each sample was normalized relative to the CA signal in the second fraction. The data show the mean signals and ranges of *2* biological replicates. (E) DLS analysis of WT IN, R269A/K273A IN, WT IN plus BI-B2, and WT IN plus BI-D. The data are representative of the results of two independent experiments.

low-oligomeric-state protein that is selectively impaired for RNA binding and is likely localized outside the CA lattice (Fig. 5B). While ALLINI-treated WT IN does not interact with viral RNA (4), the large sizes of IN-ALLINI complexes observed in DLS experiments (Fig. 5E) are fully consistent with IN from ALLINI-treated virions migrating in the dense sucrose fractions.

NC-RNA interactions are not altered in eccentric particles. NC has been proposed to regulate the maturation of the genomic RNA dimer in particles and to ensure the specificity and efficiency of reverse transcription (45). Therefore, we reasoned that modulation of the binding pattern of NC on vRNAs in eccentric particles might contribute to the reverse transcription defect in target cells. To test this possibility, we conducted NC UV cross-linking immunoprecipitation and sequencing (CLIP-seq) experiments on HIV-1_{NL4-3} particles generated in the presence of BI-B2, as well as on a

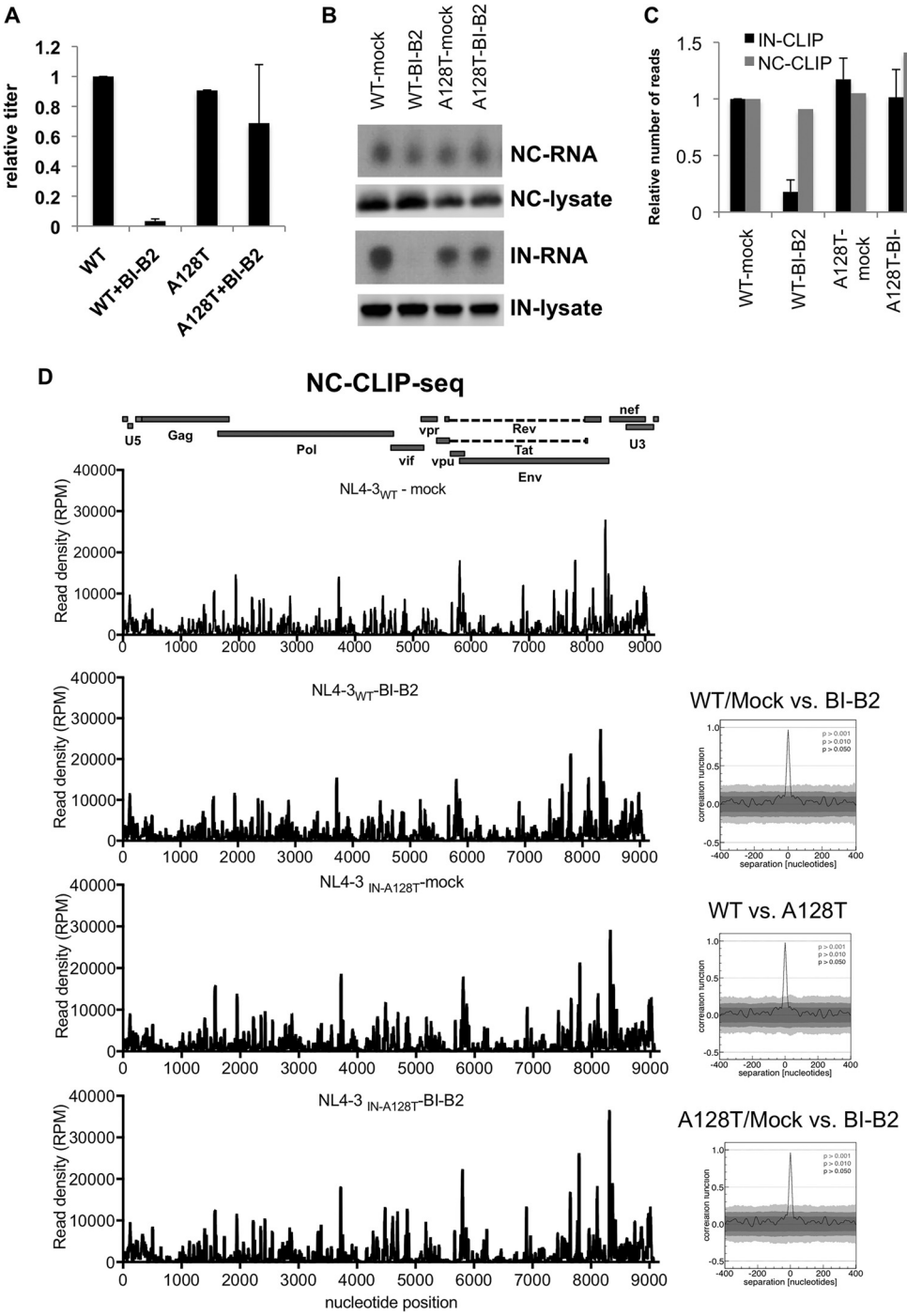

FIG 6 NC-RNA interactions are not altered in eccentric particles. (A) Infectious titers of mock- and BI-B2-treated HIV-1_{WT} and HIV-$1_{IN\ A128T}$ particles were determined on NIH-TZM reporter cells and normalized relative to mock-treated HIV-$1_{NL4\text{-}3WT}$ particles. The titers are means and SD; $n = 3$ independent experiments. (B) Representative autoradiogram of NC-RNA and IN-RNA adducts isolated from mock- and BI-B2-treated HIV-$1_{NL4\text{-}3\ WT}$ and HIV-$1_{NL4\text{-}3\ IN\ A128T}$ particles. Corresponding Western blot analyses of NC and IN in virus lysates are shown below the autoradiograms. (C) The normalized number of reads that mapped to viral RNAs obtained from 2 independent IN-CLIP-seq experiments and one NC-CLIP-seq experiment are shown relative to experiments conducted on WT particles. (D) NC CLIP-seq results showing read densities (RPM) that mapped to the viral genome obtained from the indicated viruses and treatments. A colinear diagram of HIV-1 genome features is shown above. Correlation analyses of data sets are represented on the right.

HIV-$1_{NL4\text{-}3\ A128T\ IN}$ mutant that is markedly resistant to BI-B2 (Fig. 6A) (43). In line with previous findings (4), similar amounts of NC-RNA complexes were immunoprecipitated from mock- and BI-B2-treated HIV-$1_{NL4\text{-}3}$ and HIV-$1_{NL4\text{-}3\ A128T\ IN}$ particles (Fig. 6B). In contrast, the binding of WT, but not A128T IN, to RNAs was dramatically reduced upon

BI-B2 treatment (Fig. 6B). Sequencing of NC- and IN-bound RNAs revealed that neither the fraction of reads that mapped to the viral genome (Fig. 6C) nor the binding pattern of NC on vRNAs (Fig. 6D) was affected in eccentric particles. In contrast, IN binding to vRNA was significantly reduced upon BI-B2 treatment of the WT (Fig. 6B and C), but not the A128T IN mutant (Fig. 6B and C). These results show that despite the mislocalization of NC-RNA complexes (4, 9, 17), the footprint of NC on vRNAs is maintained in the eccentric particles.

Eccentric cores can efficiently saturate restricting TRIM5 molecules. As a significant fraction of eccentric particles contain aberrantly formed and nonconical CA assemblies (17), we next wanted to determine whether they still retain features that can be recognized by restricting TRIM5 molecules in cells. To this end, we performed abrogation-of-restriction assays (36, 46), which rely on the saturation of restricting TRIM5 proteins by increasing doses of TRIM5-sensitive capsids, resulting in infection by viruses that would otherwise be restricted. pgsA-derived cells expressing rhesus macaque TRIM5α (rhTRIM5α) or owl monkey TRIMCyp (omkTRIMCyp) were infected simultaneously with increasing amounts of VSV-G-pseudotyped WT or eccentric HIV-1 particles carrying a minimal viral genome (47) or full-length viral genomes (NL4-3) and a fixed amount of WT green fluorescent protein (GFP) reporter virus. As negative controls, we included the CA-LMNEIE (48) and CA-G89V (49) mutants, which confer resistance to rhTRIM5α and omkTRIMCyp proteins, respectively.

HIV-1_{WT} and HIV-$1_{IN\ R269A/K273A}$ particles containing minimal viral genomes abrogated rhTRIM5α (Fig. 7A) and omkTRIMCyp (Fig. 7B) restriction at similar efficiencies, as indicated by the equivalent increases in the titer of a WT GFP reporter virus. In contrast, HIV-$1_{LMNEIE\ CA}$ and HIV-$1_{G89V\ CA}$ viruses failed to abrogate restriction by rhTRIM5α (Fig. 7A) and omkTRIMCyp (Fig. 7B), respectively. Importantly, similar results were obtained using full-length HIV-1_{NL4-3} and HIV-$1_{NL4-3\ IN\ R269A/K273A}$ (Fig. 7C and D), suggesting that the choice of viral genome in these experiments did not alter the biochemical effects of the R269A/K273A IN mutation on particle formation. Finally, eccentric particles generated in the presence of BI-B2 and BI-D abrogated rhTRIM5α (Fig. 7D) and omkTRIMCyp (Fig. 7E) proteins, albeit at a modestly lower efficiency than mock-treated particles. This can be attributed in part to ALLINI-mediated inhibition of integration in target cells due to carryover of ALLINIs in the virus inoculum. Collectively, these results indicate that the CA assemblies in eccentric particles still largely retain features that can saturate TRIM5 molecules in infected cells.

CA assemblies in eccentric particles can be degraded by omkTRIMCyp. We next wanted to extend these observations and asked whether CA assemblies in eccentric particles can be targeted for degradation by the omkTRIMCyp protein. In the next set of experiments, we primarily focused on HIV-$1_{IN\ R269A/K273A}$ particles, as the fates of viral components in target cells were identical to those of ALLINI-treated particles (Fig. 1 to 3). pgsA-omkTRIMCyp and nonrestricting pgsA-huTRIM5α cells were infected with HIV-1_{WT} and HIV-$1_{IN\ R269A/K273A}$ in parallel, and postnuclear material was analyzed as described above.

As revealed by the similar migration patterns and quantities of CA and IN, virion binding to cells was equivalent under all conditions immediately after synchronization of infections ($T = 0$) (Fig. 8A). At 2 h postinfection with WT viruses ($T = 2$ h), the presence of omkTRIMCyp led to the expected disappearance of CA, IN (Fig. 8B), vRNA (Fig. 8C), and cDNA (Fig. 8D) from the dense fractions without any concurrent increase in the top fractions. In line with the saturation experiments, CA from HIV-$1_{IN\ R269A/K273A}$ particles was similarly degraded by the omkTRIMCyp protein (Fig. 8B). Degradation of IN (Fig. 8B) and vRNA (Fig. 8C) following infection of omkTRIMCyp cells with HIV-$1_{IN\ R269A/K273A}$ is likely due to an omkTRIMCyp-independent mechanism, as observed in huTRIM5α cells. As expected, cDNA synthesis was impaired in huTRIM5α cells infected with HIV-$1_{IN\ R269A/K273A}$ (Fig. 8D). The presence of omkTRIMCyp led to a further decrease in reverse transcription products (Fig. 8D), likely suggesting the presence of a small fraction of particles with WT morphology in the virus popula-

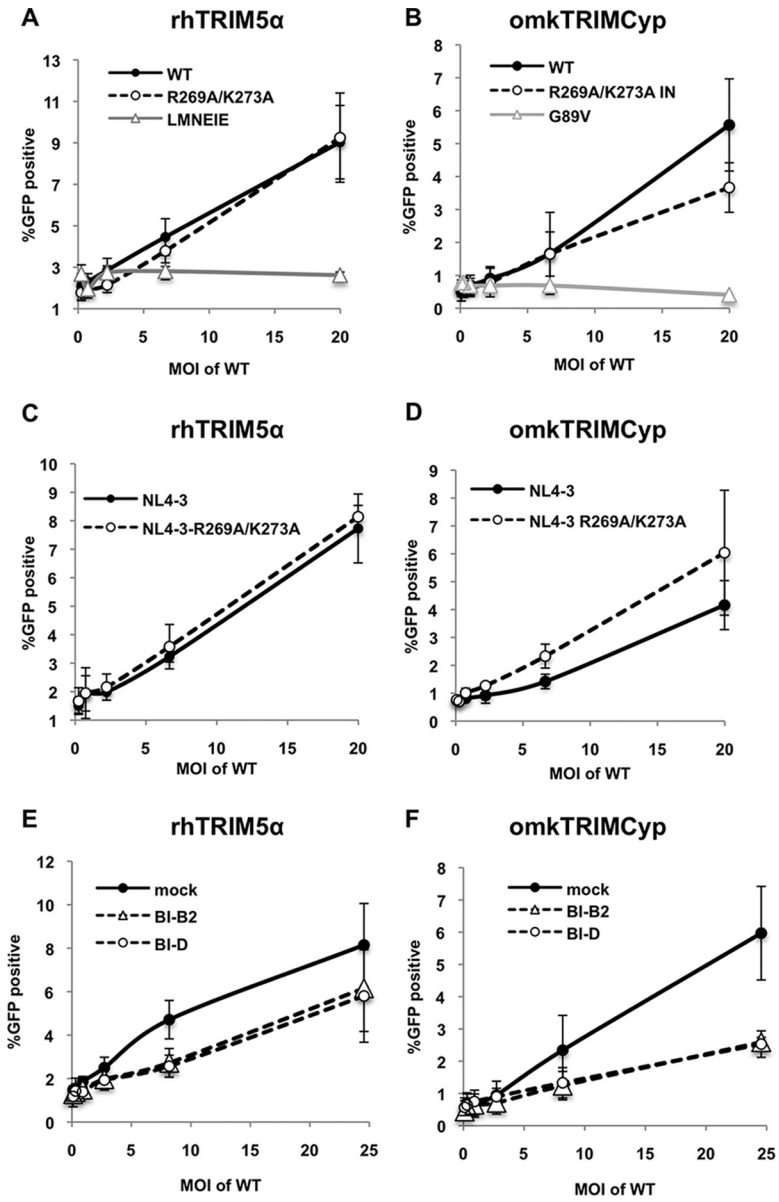

FIG 7 Eccentric particles efficiently saturate restricting TRIM5 proteins. Eccentric particles generated by IN R269A/K273A mutation (NLGP and NL4-3 backbone) or BI-B2 or BI-D treatment, along with rhTRIM5α-resistant CA-LMNEIE mutants (NLGP backbone) and omkTRIMCyp-resistant CA-G89V mutants (NLGP backbone), were tested for the ability to saturate rhTRIM5α (A, C, and E) and omkTRIMCyp (B, D, and F). Cells were infected with the indicated VSV-G-pseudotyped abrogating viruses simultaneously with a fixed amount of WT GFP reporter virus. The titers of the abrogating viruses were determined on NIH-TZM cells. The MOI of WT- and mock-treated viruses are indicated on the *x* axes. The viral inoculum for eccentric particles was normalized to that of WT/mock-treated viruses based on RT activity. The percentages of GFP-positive cells were determined 2 days postinfection by FACS and are shown on the *y* axes. The data represent the averages of the results of two independent experiments. The error bars show the ranges. Similar results were obtained from two other independent experiments done under similar conditions.

tion, as observed previously (17). Notably, while similar levels of RT activity were present in dense sucrose fractions for WT and IN R269A/K273A mutant viruses under nonrestrictive conditions, the presence of omkTRIMCyp led to a significant decrease in RT activity in these fractions (Fig. 8E). We noted a second peak of RT activity in the top (1 to 4) sucrose fractions for WT particles (Fig. 1I, 3I, and 8E). As this population of RT is insensitive to omkTRIMCyp restriction and does not comigrate with other viral components, it likely represents soluble RT molecules that are not associated with

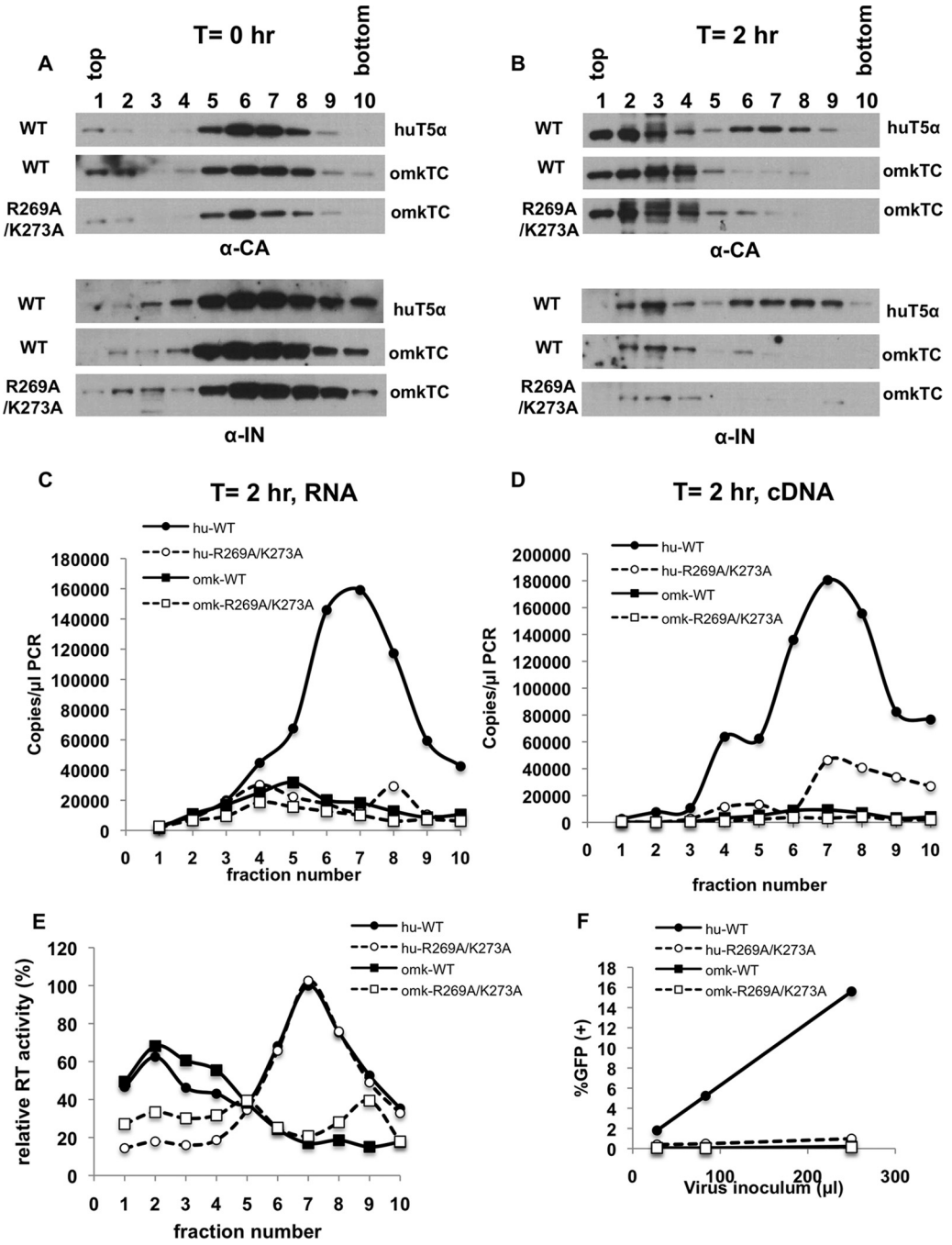

FIG 8 Eccentric cores generated through IN R269A/K273A mutation can be efficiently degraded by omkTRIMCyp. pgsA-huTRIM5α and pgsA-omkTRIMCyp cells were infected with VSV-G-pseudotyped HIV-1_{WT} or HIV-$1_{IN\ R269A/K273A}$. Infected cells were processed at 0 h and 2 h as described in Materials and Methods. (A and B) Western blot analysis of CA (p24) and IN in fractions collected from 0-h (A) and 2-h (B) samples. (C to E) Q-PCR analysis of viral RNA (C), viral cDNA (D), and RT activity (E) in fractions collected from 2-h samples. Peak RT activity (i.e., in the 7th fraction) of huTRIM5α-WT samples was set to 100%. (F) Virus titers on pgsA-huTRIM5α and pgsA-omkTRIMCyp cells infected in parallel were determined by FACS 2 days postinfection. The data are representative of the results of two independent experiments.

vRNPs. As expected, degradation of viral components was associated with a severe infectivity defect downstream (Fig. 8F). Overall, these findings reinforce the conclusion that RT remains associated with CA in eccentric particles and suggest that TRIM5 can recognize and degrade the nonconical CA assemblies and the associated RT molecules.

Similar results were observed for ALLINI-treated particles; viral CA from eccentric cores generated by BI-B2 and BI-D treatment was efficiently degraded by omkTRIMCyp

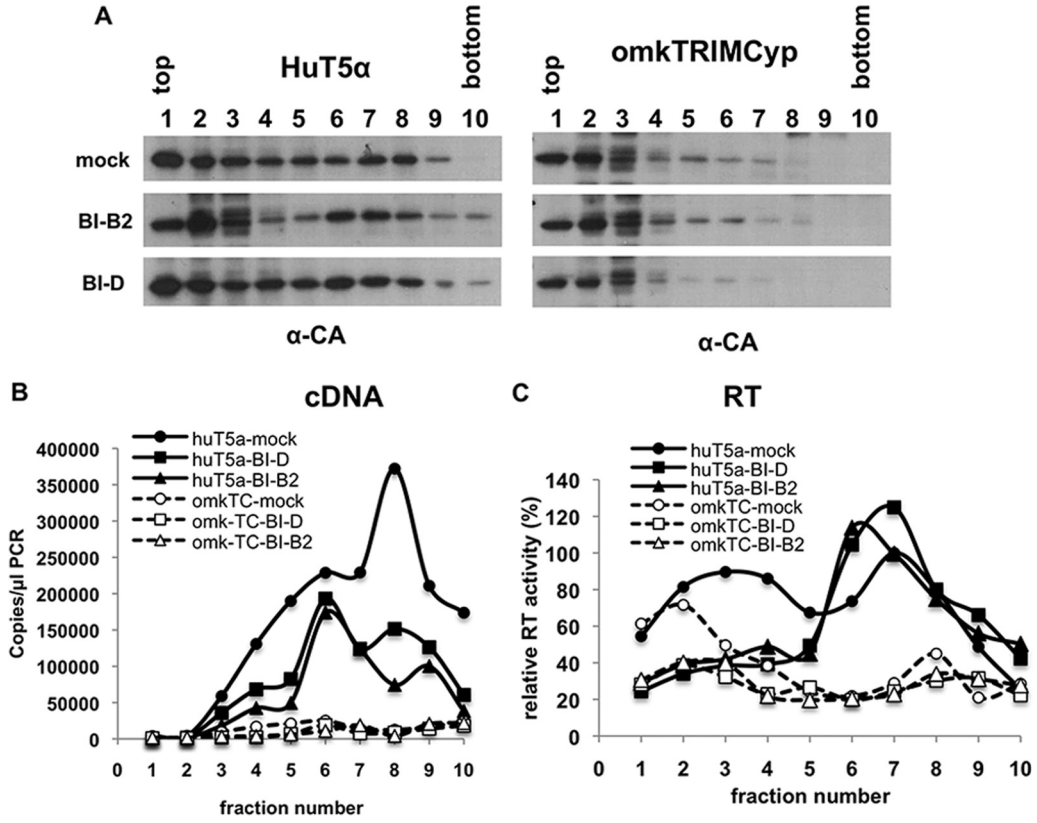

FIG 9 Eccentric cores generated in the presence of ALLINIs can be efficiently degraded by omkTRIMCyp. pgsA-huTRIM5α and pgsA-omkTRIMCyp cells were infected with mock-, BI-B2-, and BI-D-treated particles. The infected cells were processed at 2 h as explained in Materials and Methods. Western blot analysis of CA (A) and Q-PCR analysis of viral cDNA (B) and RT activity (C) in the collected fractions are shown. RT activity in the 7th fraction of mock-treated samples in huTRIM5α cells was set to 100%. The data are representative of the results of two independent experiments.

(Fig. 9A). Likewise, while ALLINI treatment reduced the amount of viral cDNA in dense fractions, the presence of omkTRIMCyp led to a further decrease (Fig. 9B). Notably, although ALLINI treatment did not affect the migration behavior or amount of RT, omkTRIMCyp led to its complete loss from dense fractions (Fig. 9C). Overall, these results show that the viral CA, together with associated RT, in eccentric particles can be efficiently recognized and degraded by a restricting TRIM5 protein.

The viral RNA genome and IN from the eccentric particles are degraded in a proteasome-independent manner. It has been proposed that the IN protein is inherently unstable due to the presence of an N-terminal phenylalanine residue that leads to its proteasomal degradation (50). Likewise, we reasoned that degradation of NC in the cytosol may subsequently expose the vRNA for further degradation. To test these possibilities, we conducted assays similar to those described above in pgsA-huTRIM5α cells in the presence of the proteasome inhibitor MG132. As expected, the migration patterns and amounts of CA in WT and eccentric particles were largely unaffected upon MG132 treatment (Fig. 10A). However, MG132 treatment did not restore IN (Fig. 10B), vRNA (Fig. 10C), or cDNA (Fig. 10D) in sucrose fractions and as a result did not rescue the defect in infectivity (Fig. 10E) of HIV-$1_{IN\ R269A/K273A}$.

Importantly, parallel experiments conducted in omkTRIMCyp cells indicated that degradation of CA (Fig. 11A) and RT (Fig. 11B) can be rescued upon MG132 treatment for both WT and eccentric particles. Although MG132 treatment restored IN (Fig. 10C), vRNA (Fig. 11D), and cDNA (Fig. 11E) for HIV-1_{WT} in omkTRIMCyp cells, it modestly, if at all, restored these components for HIV-$1_{IN\ R269A/K273A}$. As previously noted (42), MG132 treatment did not restore virion infectivity of HIV-1_{WT} and HIV-$1_{IN\ R269A/K273A}$ particles in omkTRIMCyp cells (Fig. 11F). In summary, these results indicated that the RNA

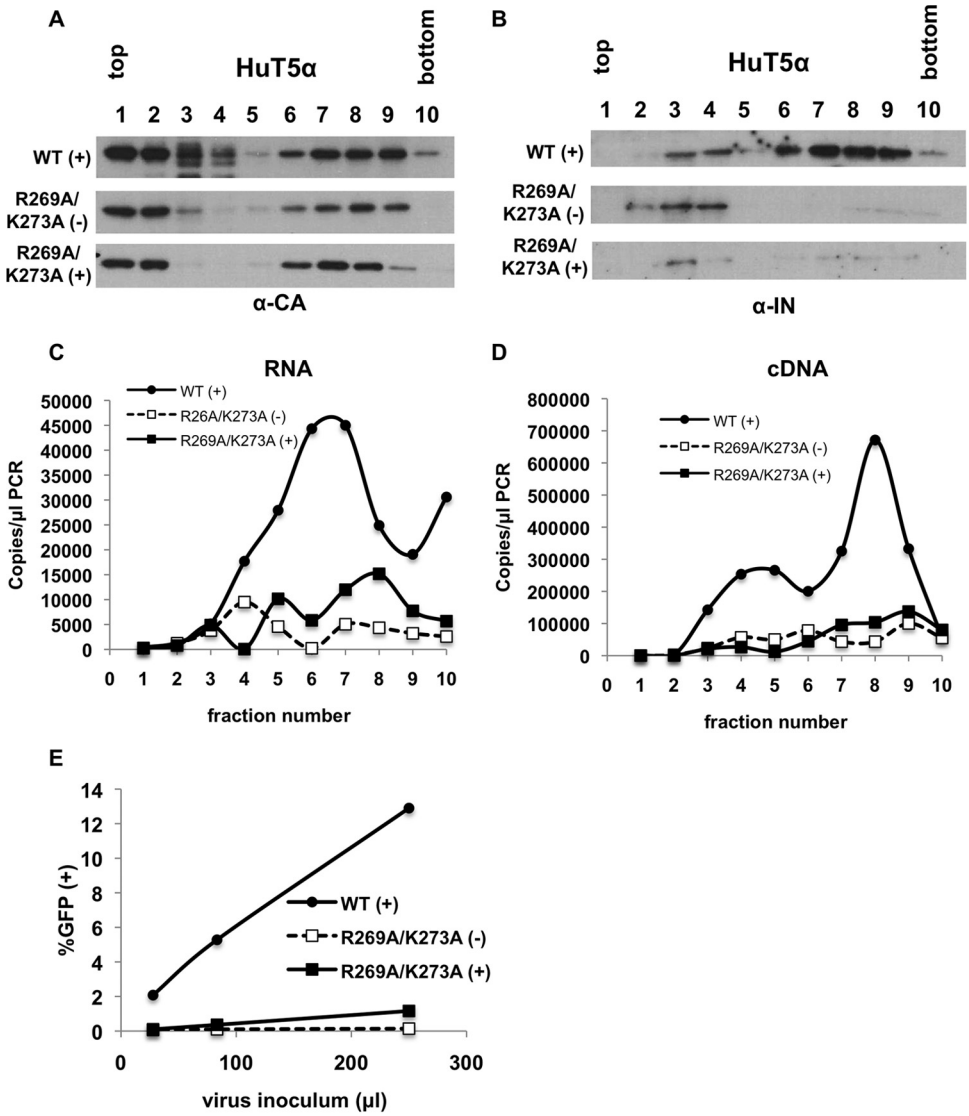

FIG 10 Inhibition of proteasomes does not rescue the degradation of eccentric core components in huTRIM5α-expressing cells. pgsA-huTRIM5α cells were infected in parallel by VSV-G-pseudotyped HIV-1_{WT} or HIV-$1_{IN\ R269A/K273A}$ in the absence or presence of 2 μM MG132. The infected cells were processed at 2 h as explained in Materials and Methods. (A to D) Western blot analysis of CA (A) and IN (B) and Q-RT-PCR analysis of viral RNA (C) and cDNA (D) in fractions collected from 2-h samples. (E) Virus titers were determined in parallel on pgsA-huTRIM5α cells by FACS. The data are representative of the results of two independent experiments.

genome and IN from the eccentric particles are degraded in a proteasome-independent manner under both nonrestricting and restricting conditions. In contrast, omkTRIMCyp-mediated degradation of CA and RT from the eccentric virions is dependent on proteasomes.

DISCUSSION

Our findings shed light on how inhibition of IN-RNA interactions by ALLINI treatment or through mutagenesis of IN alters the fates of multiple HIV-1 core components in virions and in target cells. We propose that IN binding to the viral RNA genome during particle maturation ensures the incorporation of both vRNPs and IN in the conical CA lattice. Inhibition of these interactions either directly by the R269A/K273A IN substitutions or indirectly by ALLINI-induced aberrant IN multimerization leads to mislocalization of vRNPs (9, 17) and possibly also IN in virions. These profound changes do not affect the degree or the pattern of NC binding on vRNAs (Fig. 6), reflecting the

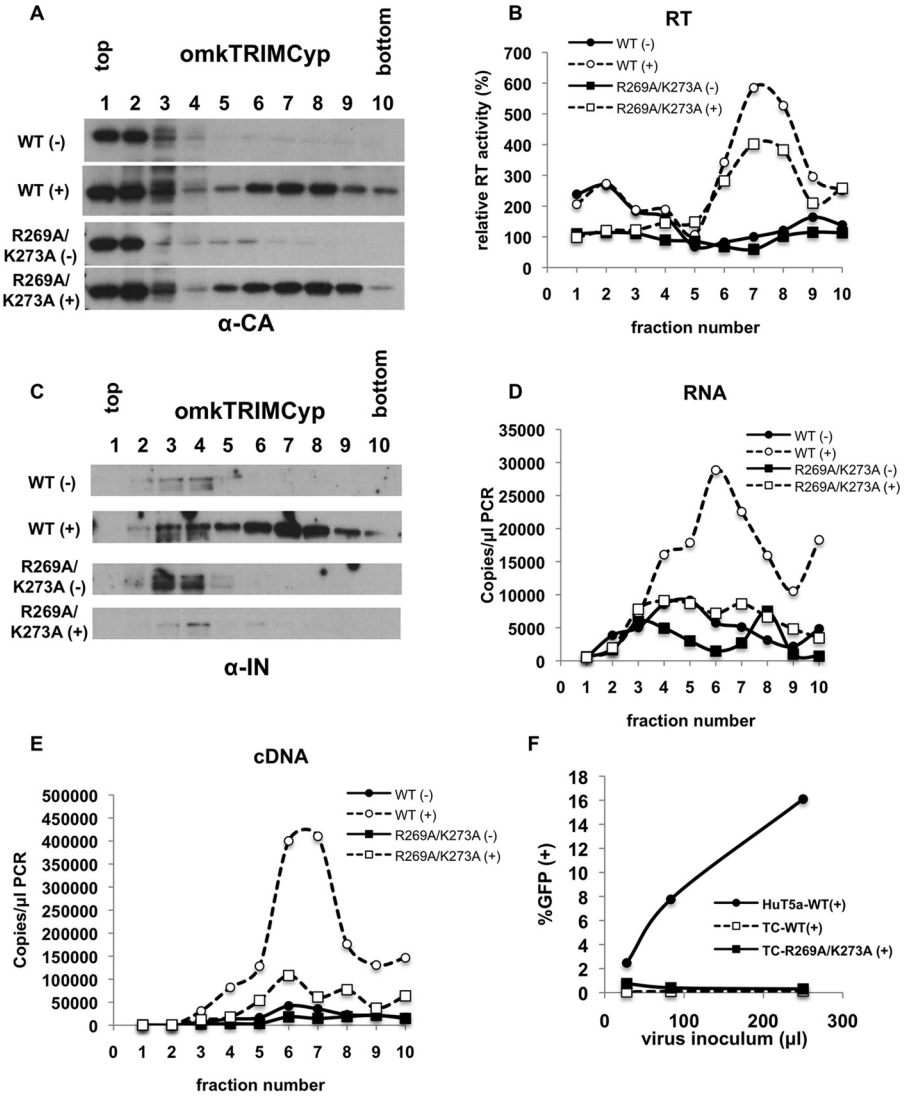

FIG 11 Inhibition of proteasomes does not rescue the degradation of vRNA and IN but restores CA and RT in omkTRIMCyp cells. pgsA-omkTRIMCyp cells were infected in parallel with VSV-G-pseudotyped HIV-1_{WT} or HIV-$1_{IN\ R269A/K273A}$ in the absence or presence of 2 μM MG132. The infected cells were processed at 2 h as explained in Materials and Methods. (A to E) Western blot analysis of CA (A) and IN (C) and Q-PCR analysis of RT activity (B), viral RNA (D), and cDNA (E) in fractions collected from 2-h samples. RT activity in the 7th fraction of WT samples in omkTRIMCyp cells was set to 100%. (F) Virus titers were determined in parallel on pgsA-huTRIM5α and pgsA-omkTRIMCyp cells by FACS. The data are representative of the results of two independent experiments.

formation of vRNP condensation prior to and independently of the formation of the core (51, 52). Most notably, while vRNA and IN in eccentric particles are subsequently prematurely degraded, similar levels of RT remain associated with CA assemblies in WT and eccentric particles upon infection of target cells. Altogether, we propose that premature degradation of the viral RNA genome in target cells, coupled with separation of RT from the eccentrically localized vRNPs, accounts for the reverse transcription block of eccentric particles (Fig. 12).

Our findings suggest that exposed vRNA is degraded in target cells with a half-life of $<$2 h. This correlates with a similarly high decay rate seen for mammalian mRNAs (53). It has been proposed that the AU-rich nucleotide content may destabilize HIV-1 RNAs following their synthesis (54–56), much like several other cellular mRNAs encoding cytokines and growth factors (57). It is unknown whether similar mechanisms can operate on eccentrically located vRNAs or if other specific antiviral molecules target

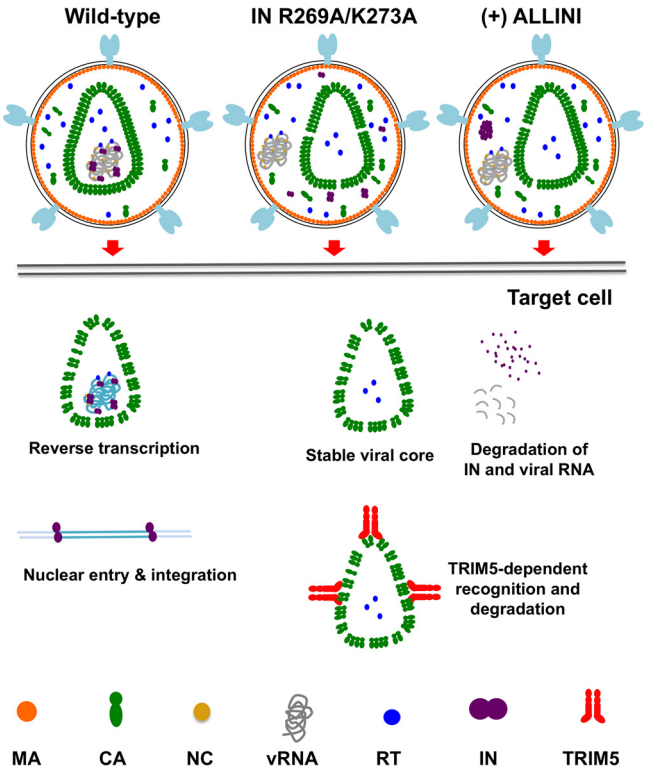

FIG 12 Schematic model of how inhibition of IN-RNA interactions alters the core morphology and fates of core components in target cells.

vRNAs for degradation. As a corollary, our findings imply that vRNAs in WT particles may be inaccessible to host cell RNA metabolism or defense pathways in infected cells due to their retention within the CA lattice. In line with this, it has recently been proposed that HIV-1 reverse transcription products, but not vRNA, can be recognized by the cytosolic DNA sensors cGAS and IFI16, likely as a result of uncoating of the CA core following cDNA synthesis (58–61). Eccentric particles will provide a unique tool to study whether incoming vRNAs contain sequence and structural features that can be recognized by cytosolic RNA sensors and whether the CA lattice prevents access of cytosolic sensors to vRNAs.

Density-based separation of core components generated in the presence of ALLINI, GS-B, has previously indicated that IN and RT cofractionate with CA (24), implying that IN and RT may still be retained inside the cores. Similarly, our results show that upon separation, IN in ALLINI-treated particles migrated toward denser sucrose fractions (Fig. 5D), although differences between the migration patterns of BI-D- and BI-B2-treated IN were noticeable (Fig. 5D). In contrast, the IN R269A/K273A mutant primarily migrated in soluble fractions (Fig. 5D). The differences between these migration patterns can be explained by the formation of IN multimers of various sizes induced upon ALLINI treatment, as revealed by DLS experiments (Fig. 5E). Nevertheless, both the ALLINI-treated IN and the IN R269A/K273A mutant are subsequently degraded in target cells. While we cannot exclude the possibility that ALLINIs and the R269A/K273A substitutions directly affect the stability of IN in target cells, our results imply that IN is either mislocalized in or loosely associated with the CA lattice in eccentric virions. Although our studies do not assign a direct role for IN in reverse transcription, it is noteworthy that IN has been previously shown to associate with reverse transcription complexes (62), which could be mediated by vRNA or direct IN-RT interactions (63). Collectively, the present findings, together with previous reports, argue strongly for a critical role of IN in the correct localization of vRNPs within the protective CA lattice for subsequent productive reverse transcription in the target cells.

Our results indicate that RT remains associated with viral CA in cells infected with eccentric particles. A small fraction of RT molecules are likely still positioned on the eccentrically localized vRNA genome. Nevertheless, as reverse transcription involves multiple template-switching events on a highly structured template (64), multiple RT molecules are required to complete reverse transcription (65). As such, we propose that in addition to the rapid degradation of vRNPs, the spatial separation of RT from the vRNA genome explains the reverse transcription defect of eccentric particles.

Cores isolated from eccentric virus particles were shown to sediment more slowly due to the mislocalization of vRNPs outside the core (24, 26). In addition, a large fraction of eccentric particles contain nonconical aberrantly formed cores (17), which may contribute to their slow migration in sucrose gradients. While our findings with detergent-treated particles are in line with these previous studies (Fig. 5A), we have observed that the migration patterns of CA isolated from cells infected with WT and eccentric particles (i.e., Fig. 1D and G, 2A and D, 3D and G, 9A, 10A, and 11A) are similar. One explanation for this difference is that separation of cytosolic material in infected cells is based on size but not density. As such, it is plausible that the size of the CA lattice in eccentric particles is similar to that in WT particles despite the morphological aberrations. Alternatively, the WT cores and the CA lattice in eccentric particles undergo similar levels of uncoating in target cells and subsequently migrate in similar patterns.

Previous studies have demonstrated a general association between the stability of CA cores and reverse transcription in infected cells (30–35). According to the currently accepted models, viral cores exist in a metastable state in virions and "uncoat" in target cells as a result of reverse transcription (66). Conversely, inhibition of reverse transcription can prevent uncoating in infected cells (28, 29). Although reverse transcription is impaired in eccentric particles, we did not observe a difference in the migration behavior or quantity of CA in dense fractions between eccentric and WT particles. Interestingly, some of the CA mutations that alter core stability have been reported to cause similar morphological defects in particle formation with condensed vRNPs juxtaposed near the viral membrane (30, 32, 33, 67–69). As such, we predict that degradation of vRNAs, and perhaps other core components, may similarly account for the reverse transcription defect of particles with altered core stabilities.

It is well established that TRIM5 restriction factors recognize features that exist not in CA monomers, but in the assembled viral CA lattice (36–39). On the other hand, formation of a conical core is not likely to be necessary for TRIM5 binding, as TRIM5 can form a hexameric supralattice on CA-NC tubes *in vitro* (41), a CA-NC cleavage mutant that cannot form conical capsids can still saturate TRIM5 restriction (40), and TRIM5-mediated restriction has been shown to require a small fraction of CA subunits (70). Importantly, virus-like particles containing only Gag and protease were found to saturate TRIM5 restriction, albeit at a lower efficiency than WT particles (36). In line with these previous studies, our findings indicate that despite the reported morphological aberrations (17), CA proteins in eccentric particles must still be arranged in a hexagonal lattice and retain features that can be recognized and degraded by a restricting TRIM5 protein (Fig. 7, 8, 9, and 11).

We have previously shown that TRIM5-mediated restriction involves proteasome-mediated degradation of CA, IN, and viral nucleic acids (42). We now show that TRIM5 restriction also leads to the degradation of RT protected within CA assemblies in a proteasome-dependent manner (Fig. 8, 9, and 11). As such, while our data do not provide conclusive evidence as to whether TRIM5 restriction primarily requires degradation or disassembly of viral cores, they suggest that all of the components of the viral cores are degraded either actively or due to their inherent instability upon TRIM5 restriction.

Overall, our findings reveal that IN-RNA interactions during virion morphogenesis ensure the correct localization of vRNA and IN inside the CA lattice to protect the viral RNA genome and IN from premature degradation during subsequent infection of the target cells. Conversely, the lack of IN binding to RNA leads to reduced stability of the viral RNA genome in target cells, as well as the spatial separation between RT and

vRNPs, which together result in the block of reverse transcription. Collectively, these studies provide key insight into the mode of action of ALLINIs and elucidate the mechanisms by which IN-RNA interactions regulate particle maturation and influence subsequent early viral postentry processes.

MATERIALS AND METHODS

Cells, viruses, and infections. CHO K1-derived pgsA-745 cells (CRL-2242; ATCC) and all of their derivatives expressing human TRIM5α, rhesus macaque TRIM5α, and owl monkey TRIMCyp were described previously (42) and were maintained in Ham's F12 medium (Life Technologies; 11765-054) supplemented with 10% fetal bovine serum and 1 mM L-glutamine. HeLa-derived TZM-bl cells (NIH AIDS Reagent Program) and HEK 293T cells (ATCC CRL-11268) were maintained in Dulbecco's modified Eagle's medium supplemented with 10% fetal bovine serum. MT-4 cells were maintained in RPMI medium supplemented with 10% fetal bovine serum. Vesicular stomatitis virus G protein (VSV-G)-pseudotyped viruses were produced by transfection of 293T cells with plasmids expressing HIV-1 NL4-3-derived Gag-Pol (pNLGP), the V1B packageable vector genome (47, 71), or the CCGW vector genome carrying GFP (36, 46) and VSV-G at a ratio of 5:5:1, respectively, using polyethyleneimine (PolySciences, Warrington, PA) as described previously (72). In some experiments, cell culture medium on transfected 293T cells was replenished with 10 μM BIB-B2- and BI-D-containing medium to generate particles with eccentric morphologies. MT-4 cells were infected with VSV-G-pseudotyped full-length NL4-3$_{WT}$ or NL4-3$_{R269A/K273A}$ synchronously at 4°C in the presence of nevirapine. Following the removal of the virus inoculum, the cells were washed extensively with 1× phosphate-buffered saline (PBS) and incubated at 37°C for 2, 5, or 24 h prior to the collection of total cellular RNA with TRIzol (Life Technologies).

Plasmids. Construction of the proviral plasmid V1B, which expresses a minigenome under the cytomegalovirus (CMV) promoter and retains viral sequences bound by IN, such as TAR and RRE, has been described previously (47, 71). The vector genome plasmid CCGW carrying a GFP reporter under the control of the CMV promoter was described previously (36, 46). The HIV-1$_{NL4-3}$-derived HIV-1 Gag-Pol sequence was inserted into the pCR/V1 plasmid (pNLGP) and was described previously (47). A pCR/V1-based NLGP expression plasmid carrying the IN R269A/K273A and CA G89V mutations was generated by transferring sequences containing the mutations from an NL4-3-based plasmid using conventional molecular biology tools. The NLGP-CA LMNEIE plasmid was previously described (48). HIV-1$_{NL4-3}$-derived proviral plasmids containing IN R269A/K273A and IN A128T mutations were described previously (4).

Analysis of virion core components in infected cells. Biochemical analysis of retroviral cores in infected cells was performed as described previously (42). Briefly, pgsA745 cells stably expressing huTRIM5α or omkTRIMCyp were infected with VSV-G-pseudotyped single-cycle GFP reporter viruses or their derivatives synchronously at 4°C. Following removal of the virus inoculum and extensive washes with 1× PBS, the cells were incubated at 37°C for 2 h. For analysis of viral RNAs, 25 μM nevirapine was included throughout the infections. In other experiments, 2 μM MG132 was included for inhibition of proteasomal degradation. Cytosolic extracts were separated by ultracentrifugation on 10 to 50% sucrose gradients using an SW50.1 rotor at 30,000 rpm for 1 h. Ten 500-μl fractions from the top of the gradient were collected, and CA, IN, vRNA, and DNA in each fraction were analyzed as previously described (42). A SYBR green-based Q-PCR assay (73) was employed to determine reverse transcriptase activity in the collected sucrose fractions. RT activity in the fractions was normalized relative to the highest level of activity (in fraction 6 or 7) of the WT or mock-treated viruses.

Equilibrium density sedimentation of virion core components *in vitro*. 293T cells grown on 15-cm dishes were transfected, and cell-free virions collected from the cell culture supernatants were pelleted through a 20% sucrose cushion. The pelleted virus particles were resuspended in 1× PBS and treated with 0.5% Triton X-100 for 2 min at room temperature. Immediately thereafter, samples were layered on top of 30 to 70% linear sucrose gradients in 1× STE buffer (100 mM NaCl, 10 mM Tris-Cl [pH 8.0], 1 mM EDTA) and centrifuged for 16 h at 4°C and 28,500 rpm, using an SW55Ti rotor. Then, 500-μl fractions were collected from the top and analyzed for CA, IN, and MA by immunoblotting.

Abrogation of TRIM5 restriction assays. The titers of viruses generated as described above were determined on NIH-TZM-bl indicator cells by X-Gal (5-bromo-4-chloro-3-indolyl-β-D-galactopyranoside) staining 2 days postinfection. As the abrogating eccentric particles are noninfectious, the virus inoculum was normalized with respect to the relative reverse transcriptase activity in each virus stock by employing a Q-PCR-based RT activity assay. For viruses generated in the presence of ALLINIs, virus stocks were first pelleted by a LentiX concentrator (Clontech) to prevent carryover of ALLINIs to target TRIM5-expressing cells. pgsA-rhTRIM5α and pgsA-omkTRIMCyp cells were infected at increasing multiplicities of infection (MOI) with abrogating WT and eccentric core-containing particles simultaneously with wild-type GFP reporter virus (MOI = 1, as determined on pgsA cells). Infected cells were fixed with formaldehyde 2 days postinfection and analyzed by fluorescence-activated cell sorting (FACS).

CLIP-seq experiments. CLIP-seq experiments were conducted as described previously (74). Briefly, 293T cells transfected with proviral plasmids were grown in the presence of 4-thiouridine and treated with ALLINIs or were left untreated for 16 h prior to virus harvest. Cell culture supernatants containing virions were collected and filtered through a 0.22-μm filter and pelleted on a 20% sucrose cushion. The virus pellets were resuspended in PBS and UV cross-linked. Following lysis, IN-RNA and NC-RNA complexes were immunoprecipitated using monoclonal anti-IN and polyclonal anti-NC antibodies. Bound RNA was end labeled with [γ-^{32}P]ATP and T4 polynucleotide kinase. The isolated protein-RNA complexes were separated by SDS-PAGE, transferred to nitrocellulose membranes, and exposed to autoradiography films. Protein-RNA complexes that corresponded to IN-RNA and NC-RNA adducts were

excised from the membranes, and RNA was purified by proteinase K digestion. The RNA was sequentially ligated to 3′ and 5′ adapters, reverse transcribed, and PCR amplified, and the resulting DNA library was subjected to sequencing by Illumina platforms. The remainder of the data analysis was followed as detailed previously (74), using a FASTX toolkit (http://hannonlab.cshl.edu/fastx_toolkit) and Bowtie (75). Briefly, sequencing reads were first trimmed off the 3′ adapter, reads shorter than 15 nucleotides were filtered out, and the library was demultiplexed based on the 5′ adapter sequences using the FASTX toolkit. The sequences were then collapsed into unique reads, followed by trimming off the 5′ adapter using the FASTX toolkit. The resulting reads were mapped to the reference viral genome (pNL4-3) containing a single repeat (R) region using the Bowtie algorithm by allowing two mismatches (−v 2 −m 1). The mapping data were further normalized, taking into account the differences in library size and, subsequently, the number of mapped reads. To this end, the number of reads that mapped to each nucleotide of the viral genome was multiplied by a scaling factor to represent reads per million mapped reads (RPM). Correlation of data sets was done in a pairwise fashion as detailed previously (74).

Dynamic-light-scattering assays. Dimethyl sulfoxide (DMSO) or 5 μM ALLINI was added to 200 nM IN and incubated in a buffer containing 50 mM HEPES, pH 7.4, 2 mM dithiothreitol (DTT), 2 mM $MgCl_2$, and 1 M NaCl for 30 min at room temperature. The DLS signal was recorded using a Malvern Nano series zetasizer instrument.

ACKNOWLEDGMENTS

This work was supported by NIH grants K22AI116258, R01AI062520, and P50GM103297 (to S.B.K.) and R01AI062520 and R01AI110310 (to M.K.).

We thank Michael Malim for the monoclonal antibodies against integrase, Paul D. Bieniasz for the TRIM5-resistant CA plasmids, James Fuchs for ALLINIs, and Kasyap Tenneti for technical assistance. We are also grateful to Ross Larue for critical reading of the manuscript.

M.K.M., D.Q.L., J.E., A.N.O., D.T., and S.B.K. conceived the study, designed the experiments, and analyzed the data. P.C.K. and M.K. designed and performed DLS experiments. M.E. conducted the correlation analyses of the CLIP-seq data sets. S.B.K. supervised the work and wrote the paper with M.K.

REFERENCES

1. Sundquist WI, Krausslich HG. 2012. HIV-1 assembly, budding, and maturation. Cold Spring Harb Perspect Med 2:a006924. https://doi.org/10.1101/cshperspect.a006924.
2. Muriaux D, Mirro J, Harvin D, Rein A. 2001. RNA is a structural element in retrovirus particles. Proc Natl Acad Sci U S A 98:5246–5251. https://doi.org/10.1073/pnas.091000398.
3. Mattei S, Flemming A, Anders-Osswein M, Krausslich HG, Briggs JA, Muller B. 2015. RNA and nucleocapsid are dispensable for mature HIV-1 capsid assembly. J Virol 89:9739–9747. https://doi.org/10.1128/JVI.00750-15.
4. Kessl JJ, Kutluay SB, Townsend D, Rebensburg S, Slaughter A, Larue RC, Shkriabai N, Bakouche N, Fuchs JR, Bieniasz PD, Kvaratskhelia M. 2016. HIV-1 integrase binds the viral RNA genome and is essential during virion morphogenesis. Cell 166:1257–1268 e12. https://doi.org/10.1016/j.cell.2016.07.044.
5. Bukovsky A, Gottlinger H. 1996. Lack of integrase can markedly affect human immunodeficiency virus type 1 particle production in the presence of an active viral protease. J Virol 70:6820–6825.
6. Engelman A. 1999. In vivo analysis of retroviral integrase structure and function. Adv Virus Res 52:411–426. https://doi.org/10.1016/S0065-3527(08)60309-7.
7. Engelman A, Englund G, Orenstein JM, Martin MA, Craigie R. 1995. Multiple effects of mutations in human immunodeficiency virus type 1 integrase on viral replication. J Virol 69:2729–2736.
8. Johnson BC, Metifiot M, Ferris A, Pommier Y, Hughes SH. 2013. A homology model of HIV-1 integrase and analysis of mutations designed to test the model. J Mol Biol 425:2133–2146. https://doi.org/10.1016/j.jmb.2013.03.027.
9. Jurado KA, Wang H, Slaughter A, Feng L, Kessl JJ, Koh Y, Wang W, Ballandras-Colas A, Patel PA, Fuchs JR, Kvaratskhelia M, Engelman A. 2013. Allosteric integrase inhibitor potency is determined through the inhibition of HIV-1 particle maturation. Proc Natl Acad Sci U S A 110:8690–8695. https://doi.org/10.1073/pnas.1300703110.
10. Mohammed KD, Topper MB, Muesing MA. 2011. Sequential deletion of the integrase (Gag-Pol) carboxyl terminus reveals distinct phenotypic classes of defective HIV-1. J Virol 85:4654–4666. https://doi.org/10.1128/JVI.02374-10.
11. Lu R, Limon A, Devroe E, Silver PA, Cherepanov P, Engelman A. 2004. Class II integrase mutants with changes in putative nuclear localization signals are primarily blocked at a postnuclear entry step of human immunodeficiency virus type 1 replication. J Virol 78:12735–12746. https://doi.org/10.1128/JVI.78.23.12735-12746.2004.
12. Lu R, Ghory HZ, Engelman A. 2005. Genetic analyses of conserved residues in the carboxyl-terminal domain of human immunodeficiency virus type 1 integrase. J Virol 79:10356–10368. https://doi.org/10.1128/JVI.79.16.10356-10368.2005.
13. Limon A, Devroe E, Lu R, Ghory HZ, Silver PA, Engelman A. 2002. Nuclear localization of human immunodeficiency virus type 1 preintegration complexes (PICs): V165A and R166A are pleiotropic integrase mutants primarily defective for integration, not PIC nuclear import. J Virol 76:10598–10607. https://doi.org/10.1128/JVI.76.21.10598-10607.2002.
14. Leavitt AD, Robles G, Alesandro N, Varmus HE. 1996. Human immunodeficiency virus type 1 integrase mutants retain in vitro integrase activity yet fail to integrate viral DNA efficiently during infection. J Virol 70:721–728.
15. Jenkins TM, Engelman A, Ghirlando R, Craigie R. 1996. A soluble active mutant of HIV-1 integrase: involvement of both the core and carboxyl-terminal domains in multimerization. J Biol Chem 271:7712–7718. https://doi.org/10.1074/jbc.271.13.7712.
16. Shehu-Xhilaga M, Hill M, Marshall JA, Kappes J, Crowe SM, Mak J. 2002. The conformation of the mature dimeric human immunodeficiency virus type 1 RNA genome requires packaging of Pol protein. J Virol 76:4331–4340. https://doi.org/10.1128/JVI.76.9.4331-4340.2002.
17. Fontana J, Jurado KA, Cheng N, Ly NL, Fuchs JR, Gorelick RJ, Engelman AN, Steven AC. 2015. Distribution and redistribution of HIV-1 nucleocapsid protein in immature, mature, and integrase-inhibited virions: a role for integrase in maturation. J Virol 89:9765–9780. https://doi.org/10.1128/JVI.01522-15.
18. Christ F, Voet A, Marchand A, Nicolet S, Desimmie BA, Marchand D, Bardiot D, Van der Veken NJ, Van Remoortel B, Strelkov SV, De Maeyer M, Chaltin P, Debyser Z. 2010. Rational design of small-molecule inhibitors of the LEDGF/p75-integrase interaction and HIV replication. Nat Chem Biol 6:442–448. https://doi.org/10.1038/nchembio.370.
19. Fader LD, Malenfant E, Parisien M, Carson R, Bilodeau F, Landry S, Pesant

M, Brochu C, Morin S, Chabot C, Halmos T, Bousquet Y, Bailey MD, Kawai SH, Coulombe R, LaPlante S, Jakalian A, Bhardwaj PK, Wernic D, Schroeder P, Amad M, Edwards P, Garneau M, Duan J, Cordingley M, Bethell R, Mason SW, Bos M, Bonneau P, Poupart MA, Faucher AM, Simoneau B, Fenwick C, Yoakim C, Tsantrizos Y. 2014. Discovery of BI 224436, a noncatalytic site integrase inhibitor (NCINI) of HIV-1. ACS Med Chem Lett 5:422–427. https://doi.org/10.1021/ml500002n.

20. Gupta K, Brady T, Dyer BM, Malani N, Hwang Y, Male F, Nolte RT, Wang L, Velthuisen E, Jeffrey J, Van Duyne GD, Bushman FD. 2014. Allosteric inhibition of human immunodeficiency virus integrase: late block during viral replication and abnormal multimerization involving specific protein domains. J Biol Chem 289:20477–20488. https://doi.org/10.1074/jbc.M114.551119.
21. Kessl JJ, Jena N, Koh Y, Taskent-Sezgin H, Slaughter A, Feng L, de Silva S, Wu L, Le Grice SF, Engelman A, Fuchs JR, Kvaratskhelia M. 2012. Multimode, cooperative mechanism of action of allosteric HIV-1 integrase inhibitors. J Biol Chem 287:16801–16811. https://doi.org/10.1074/jbc.M112.354373.
22. Le Rouzic E, Bonnard D, Chasset S, Bruneau JM, Chevreuil F, Le Strat F, Nguyen J, Beauvoir R, Amadori C, Brias J, Vomscheid S, Eiler S, Levy N, Delelis O, Deprez E, Saib A, Zamborlini A, Emiliani S, Ruff M, Ledoussal B, Moreau F, Benarous R. 2013. Dual inhibition of HIV-1 replication by integrase-LEDGF allosteric inhibitors is predominant at the post-integration stage. Retrovirology 10:144. https://doi.org/10.1186/1742-4690-10-144.
23. van Bel N, van der Velden Y, Bonnard D, Le Rouzic E, Das AT, Benarous R, Berkhout B. 2014. The allosteric HIV-1 integrase inhibitor BI-D affects virion maturation but does not influence packaging of a functional RNA genome. PLoS One 9:e103552. https://doi.org/10.1371/journal.pone.0103552.
24. Balakrishnan M, Yant SR, Tsai L, O'Sullivan C, Bam RA, Tsai A, Niedziela-Majka A, Stray KM, Sakowicz R, Cihlar T. 2013. Non-catalytic site HIV-1 integrase inhibitors disrupt core maturation and induce a reverse transcription block in target cells. PLoS One 8:e74163. https://doi.org/10.1371/journal.pone.0074163.
25. Desimmie BA, Schrijvers R, Demeulemeester J, Borrenberghs D, Weydert C, Thys W, Vets S, Van Remoortel B, Hofkens J, De Rijck J, Hendrix J, Bannert N, Gijsbers R, Christ F, Debyser Z. 2013. LEDGINs inhibit late stage HIV-1 replication by modulating integrase multimerization in the virions. Retrovirology 10:57. https://doi.org/10.1186/1742-4690-10-57.
26. Sharma A, Slaughter A, Jena N, Feng L, Kessl JJ, Fadel HJ, Malani N, Male F, Wu L, Poeschla E, Bushman FD, Fuchs JR, Kvaratskhelia M. 2014. A new class of multimerization selective inhibitors of HIV-1 integrase. PLoS Pathog 10:e1004171. https://doi.org/10.1371/journal.ppat.1004171.
27. Gupta K, Turkki V, Sherrill-Mix S, Hwang Y, Eilers G, Taylor L, McDanal C, Wang P, Temelkoff D, Nolte RT, Velthuisen E, Jeffrey J, Van Duyne GD, Bushman FD. 2016. Structural basis for inhibitor-induced aggregation of HIV integrase. PLoS Biol 14:e1002584. https://doi.org/10.1371/journal.pbio.1002584.
28. Yang Y, Fricke T, Diaz-Griffero F. 2013. Inhibition of reverse transcriptase activity increases stability of the HIV-1 core. J Virol 87:683–687. https://doi.org/10.1128/JVI.01228-12.
29. Hulme AE, Perez O, Hope TJ. 2011. Complementary assays reveal a relationship between HIV-1 uncoating and reverse transcription. Proc Natl Acad Sci U S A 108:9975–9980. https://doi.org/10.1073/pnas.1014522108.
30. Fitzon T, Leschonsky B, Bieler K, Paulus C, Schroder J, Wolf H, Wagner R. 2000. Proline residues in the HIV-1 NH2-terminal capsid domain: structure determinants for proper core assembly and subsequent steps of early replication. Virology 268:294–307. https://doi.org/10.1006/viro.1999.0178.
31. Forshey BM, von Schwedler U, Sundquist WI, Aiken C. 2002. Formation of a human immunodeficiency virus type 1 core of optimal stability is crucial for viral replication. J Virol 76:5667–5677. https://doi.org/10.1128/JVI.76.11.5667-5677.2002.
32. Jiang J, Ablan SD, Derebail S, Hercik K, Soheilian F, Thomas JA, Tang S, Hewlett I, Nagashima K, Gorelick RJ, Freed EO, Levin JG. 2011. The interdomain linker region of HIV-1 capsid protein is a critical determinant of proper core assembly and stability. Virology 421:253–265. https://doi.org/10.1016/j.virol.2011.09.012.
33. Tang S, Murakami T, Agresta BE, Campbell S, Freed EO, Levin JG. 2001. Human immunodeficiency virus type 1 N-terminal capsid mutants that exhibit aberrant core morphology and are blocked in initiation of reverse transcription in infected cells. J Virol 75:9357–9366. https://doi.org/10.1128/JVI.75.19.9357-9366.2001.
34. Yang R, Shi J, Byeon IJ, Ahn J, Sheehan JH, Meiler J, Gronenborn AM, Aiken C. 2012. Second-site suppressors of HIV-1 capsid mutations: restoration of intracellular activities without correction of intrinsic capsid stability defects. Retrovirology 9:30. https://doi.org/10.1186/1742-4690-9-30.
35. Hulme AE, Kelley Z, Okocha EA, Hope TJ. 2015. Identification of capsid mutations that alter the rate of HIV-1 uncoating in infected cells. J Virol 89:643–651. https://doi.org/10.1128/JVI.03043-14.
36. Cowan S, Hatziioannou T, Cunningham T, Muesing MA, Gottlinger HG, Bieniasz PD. 2002. Cellular inhibitors with Fv1-like activity restrict human and simian immunodeficiency virus tropism. Proc Natl Acad Sci U S A 99:11914–11919. https://doi.org/10.1073/pnas.162299499.
37. Munk C, Brandt SM, Lucero G, Landau NR. 2002. A dominant block to HIV-1 replication at reverse transcription in simian cells. Proc Natl Acad Sci U S A 99:13843–13848. https://doi.org/10.1073/pnas.212400099.
38. Besnier C, Takeuchi Y, Towers G. 2002. Restriction of lentivirus in monkeys. Proc Natl Acad Sci U S A 99:11920–11925. https://doi.org/10.1073/pnas.172384599.
39. Dodding MP, Bock M, Yap MW, Stoye JP. 2005. Capsid processing requirements for abrogation of Fv1 and Ref1 restriction. J Virol 79:10571–10577. https://doi.org/10.1128/JVI.79.16.10571-10577.2005.
40. Shi J, Aiken C. 2006. Saturation of TRIM5 alpha-mediated restriction of HIV-1 infection depends on the stability of the incoming viral capsid. Virology 350:493–500. https://doi.org/10.1016/j.virol.2006.03.013.
41. Ganser-Pornillos BK, Chandrasekaran V, Pornillos O, Sodroski JG, Sundquist WI, Yeager M. 2011. Hexagonal assembly of a restricting TRIM5alpha protein. Proc Natl Acad Sci U S A 108:534–539. https://doi.org/10.1073/pnas.1013426108.
42. Kutluay SB, Perez-Caballero D, Bieniasz PD. 2013. Fates of retroviral core components during unrestricted and TRIM5-restricted infection. PLoS Pathog 9:e1003214. https://doi.org/10.1371/journal.ppat.1003214.
43. Feng L, Sharma A, Slaughter A, Jena N, Koh Y, Shkriabai N, Larue RC, Patel PA, Mitsuya H, Kessl JJ, Engelman A, Fuchs JR, Kvaratskhelia M. 2013. The A128T resistance mutation reveals aberrant protein multimerization as the primary mechanism of action of allosteric HIV-1 integrase inhibitors. J Biol Chem 288:15813–15820. https://doi.org/10.1074/jbc.M112.443390.
44. Briggs JA, Simon MN, Gross I, Krausslich HG, Fuller SD, Vogt VM, Johnson MC. 2004. The stoichiometry of Gag protein in HIV-1. Nat Struct Mol Biol 11:672–675. https://doi.org/10.1038/nsmb785.
45. Levin JG, Mitra M, Mascarenhas A, Musier-Forsyth K. 2010. Role of HIV-1 nucleocapsid protein in HIV-1 reverse transcription. RNA Biol 7:754–774. https://doi.org/10.4161/rna.7.6.14115.
46. Hatziioannou T, Cowan S, Goff SP, Bieniasz PD, Towers GJ. 2003. Restriction of multiple divergent retroviruses by Lv1 and Ref1. EMBO J 22:385–394. https://doi.org/10.1093/emboj/cdg042.
47. Zennou V, Perez-Caballero D, Gottlinger H, Bieniasz PD. 2004. APOBEC3G incorporation into human immunodeficiency virus type 1 particles. J Virol 78:12058–12061. https://doi.org/10.1128/JVI.78.21.12058-12061.2004.
48. Soll SJ, Wilson SJ, Kutluay SB, Hatziioannou T, Bieniasz PD. 2013. Assisted evolution enables HIV-1 to overcome a high TRIM5alpha-imposed genetic barrier to rhesus macaque tropism. PLoS Pathog 9:e1003667. https://doi.org/10.1371/journal.ppat.1003667.
49. Yoo S, Myszka DG, Yeh C, McMurray M, Hill CP, Sundquist WI. 1997. Molecular recognition in the HIV-1 capsid/cyclophilin A complex. J Mol Biol 269:780–795. https://doi.org/10.1006/jmbi.1997.1051.
50. Mulder LC, Muesing MA. 2000. Degradation of HIV-1 integrase by the N-end rule pathway. J Biol Chem 275:29749–29753. https://doi.org/10.1074/jbc.M004670200.
51. de Marco A, Muller B, Glass B, Riches JD, Krausslich HG, Briggs JA. 2010. Structural analysis of HIV-1 maturation using cryo-electron tomography. PLoS Pathog 6:e1001215. https://doi.org/10.1371/journal.ppat.1001215.
52. Pettit SC, Moody MD, Wehbie RS, Kaplan AH, Nantermet PV, Klein CA, Swanstrom R. 1994. The p2 domain of human immunodeficiency virus type 1 Gag regulates sequential proteolytic processing and is required to produce fully infectious virions. J Virol 68:8017–8027.
53. Yang E, van Nimwegen E, Zavolan M, Rajewsky N, Schroeder M, Magnasco M, Darnell JE, Jr. 2003. Decay rates of human mRNAs: correlation with functional characteristics and sequence attributes. Genome Res 13:1863–1872. https://doi.org/10.1101/gr.997703.
54. Maldarelli F, Martin MA, Strebel K. 1991. Identification of posttranscrip-

tionally active inhibitory sequences in human immunodeficiency virus type 1 RNA: novel level of gene regulation. J Virol 65:5732–5743.
55. Schwartz S, Campbell M, Nasioulas G, Harrison J, Felber BK, Pavlakis GN. 1992. Mutational inactivation of an inhibitory sequence in human immunodeficiency virus type 1 results in Rev-independent gag expression. J Virol 66:7176–7182.
56. Schwartz S, Felber BK, Pavlakis GN. 1992. Distinct RNA sequences in the gag region of human immunodeficiency virus type 1 decrease RNA stability and inhibit expression in the absence of Rev protein. J Virol 66:150–159.
57. Wu X, Brewer G. 2012. The regulation of mRNA stability in mammalian cells: 2.0. Gene 500:10–21. https://doi.org/10.1016/j.gene.2012.03.021.
58. Gao D, Wu J, Wu YT, Du F, Aroh C, Yan N, Sun L, Chen ZJ. 2013. Cyclic GMP-AMP synthase is an innate immune sensor of HIV and other retroviruses. Science 341:903–906. https://doi.org/10.1126/science.1240933.
59. Lahaye X, Satoh T, Gentili M, Cerboni S, Conrad C, Hurbain I, El Marjou A, Lacabaratz C, Lelievre JD, Manel N. 2013. The capsids of HIV-1 and HIV-2 determine immune detection of the viral cDNA by the innate sensor cGAS in dendritic cells. Immunity 39:1132–1142. https://doi.org/10.1016/j.immuni.2013.11.002.
60. Rasaiyaah J, Tan CP, Fletcher AJ, Price AJ, Blondeau C, Hilditch L, Jacques DA, Selwood DL, James LC, Noursadeghi M, Towers GJ. 2013. HIV-1 evades innate immune recognition through specific cofactor recruitment. Nature 503:402–405. https://doi.org/10.1038/nature12769.
61. Monroe KM, Yang Z, Johnson JR, Geng X, Doitsh G, Krogan NJ, Greene WC. 2014. IFI16 DNA sensor is required for death of lymphoid CD4 T cells abortively infected with HIV. Science 343:428–432. https://doi.org/10.1126/science.1243640.
62. Nermut MV, Fassati A. 2003. Structural analyses of purified human immunodeficiency virus type 1 intracellular reverse transcription complexes. J Virol 77:8196–8206. https://doi.org/10.1128/JVI.77.15.8196-8206.2003.
63. Tekeste SS, Wilkinson TA, Weiner EM, Xu X, Miller JT, Le Grice SF, Clubb RT, Chow SA. 2015. Interaction between reverse transcriptase and integrase is required for reverse transcription during HIV-1 replication. J Virol 89:12058–12069. https://doi.org/10.1128/JVI.01471-15.
64. Sarafianos SG, Marchand B, Das K, Himmel DM, Parniak MA, Hughes SH, Arnold E. 2009. Structure and function of HIV-1 reverse transcriptase: molecular mechanisms of polymerization and inhibition. J Mol Biol 385:693–713. https://doi.org/10.1016/j.jmb.2008.10.071.
65. Julias JG, Ferris AL, Boyer PL, Hughes SH. 2001. Replication of phenotypically mixed human immunodeficiency virus type 1 virions containing catalytically active and catalytically inactive reverse transcriptase. J Virol 75:6537–6546. https://doi.org/10.1128/JVI.75.14.6537-6546.2001.
66. Ambrose Z, Aiken C. 2014. HIV-1 uncoating: connection to nuclear entry and regulation by host proteins. Virology 454-455:371–379. https://doi.org/10.1016/j.virol.2014.02.004.
67. von Schwedler UK, Stemmler TL, Klishko VY, Li S, Albertine KH, Davis DR, Sundquist WI. 1998. Proteolytic refolding of the HIV-1 capsid protein amino-terminus facilitates viral core assembly. EMBO J 17:1555–1568. https://doi.org/10.1093/emboj/17.6.1555.
68. Reicin AS, Ohagen A, Yin L, Hoglund S, Goff SP. 1996. The role of Gag in human immunodeficiency virus type 1 virion morphogenesis and early steps of the viral life cycle. J Virol 70:8645–8652.
69. von Schwedler UK, Stray KM, Garrus JE, Sundquist WI. 2003. Functional surfaces of the human immunodeficiency virus type 1 capsid protein. J Virol 77:5439–5450. https://doi.org/10.1128/JVI.77.9.5439-5450.2003.
70. Shi J, Friedman DB, Aiken C. 2013. Retrovirus restriction by TRIM5 proteins requires recognition of only a small fraction of viral capsid subunits. J Virol 87:9271–9278. https://doi.org/10.1128/JVI.00713-13.
71. Jouvenet N, Simon SM, Bieniasz PD. 2009. Imaging the interaction of HIV-1 genomes and Gag during assembly of individual viral particles. Proc Natl Acad Sci U S A 106:19114–19119. https://doi.org/10.1073/pnas.0907364106.
72. Durocher Y, Perret S, Kamen A. 2002. High-level and high-throughput recombinant protein production by transient transfection of suspension-growing human 293-EBNA1 cells. Nucleic Acids Res 30:E9. https://doi.org/10.1093/nar/30.2.e9.
73. Pizzato M, Erlwein O, Bonsall D, Kaye S, Muir D, McClure MO. 2009. A one-step SYBR Green I-based product-enhanced reverse transcriptase assay for the quantitation of retroviruses in cell culture supernatants. J Virol Methods 156:1–7. https://doi.org/10.1016/j.jviromet.2008.10.012.
74. Kutluay SB, Zang T, Blanco-Melo D, Powell C, Jannain D, Errando M, Bieniasz PD. 2014. Global changes in the RNA binding specificity of HIV-1 gag regulate virion genesis. Cell 159:1096–1109. https://doi.org/10.1016/j.cell.2014.09.057.
75. Langmead B, Trapnell C, Pop M, Salzberg SL. 2009. Ultrafast and memory-efficient alignment of short DNA sequences to the human genome. Genome Biol 10:R25. https://doi.org/10.1186/gb-2009-10-3-r25.